Axion string dynamics I: 2+1D

To cite this article: Leesa M. Fleury and Guy D. Moore JCAP05(2016)005

View the article online for updates and enhancements.

Axion string dynamics I: 2+1D

Leesa M. Fleury[a] and Guy D. Moore[b]

[a]University of British Columbia, Department of Physics & Astronomy,
  6224 Agricultural Road, Vancouver BC V6T 1Z1, Canada

[b]Institut für Kernphysik, Technische Universität Darmstadt,
  Schlossgartenstraße 2, D-64289 Darmstadt, Germany

 E-mail: lfleury@phas.ubc.ca, guy.moore@physik.tu-darmstadt.de

Abstract. If the axion exists and if the initial axion field value is uncorrelated at causally disconnected points, then it should be possible to predict the efficiency of cosmological axion production, relating the axionic dark matter density to the axion mass. The main obstacle to making this prediction is correctly treating the axion string cores. We develop a new algorithm for treating the axionic string cores correctly in 2+1 dimensions. When the axionic string cores are given their full physical string tension, axion production is about twice as efficient as in previous simulations. We argue that the string network in 2+1 dimensions should behave very differently than in 3+1 dimensions, so this result cannot be simply carried over to the physical case. We outline how to extend our method to 3+1D axion string dynamics.

JCAP05(2016)005

doi:10.1088/1475-7516/2016/05/005

Contents

1 Introduction

The axion [1–4] is a hypothetical particle, the angular excitation of a proposed "Peccei-Quinn" (PQ) field φ that would solve the strong CP problem [5–7] while providing a viable dark matter candidate [8–10]. If PQ symmetry is restored in the early Universe (either during or after inflation), it should be possible to make a definite prediction for the axion dark matter density which would be produced cosmologically. However, the axion production is complicated by topological structures (axionic strings) which appear in the axionic field [11], and so far their dynamics have not been reliably simulated. Thus we currently lack a quantitative determination of the efficiency of axion production in this scenario, and can therefore not yet fix the relation between the axion dark matter density and the axion mass. This is unfortunate. If we could fix this relation, it would make the axion dark-matter scenario predictive and help axion search experiments [12–14] know in what frequency bandwidth to look.

The goal of this paper is to make some progress on developing the tools to study axion production in the presence of axionic strings. We will not present a complete methodology or reliable results, but we lay the groundwork for getting there by presenting an interesting algorithmic advance. We start by reviewing the relevant physics of the axion field, and clarifying the main problem. The axion field is a complex scalar φ which spontaneously breaks a U(1) (phase) symmetry. The Lagrangian density is

$$-\mathcal{L}_{\varphi_1} = \partial_\mu \varphi^* \partial^\mu \varphi + \frac{\lambda}{8} \left(2\varphi^* \varphi - f_a^2 \right)^2 , \tag{1.1}$$

invariant under $\varphi \to \varphi e^{i\theta}$, plus a small explicit breaking term, arising from QCD axions:

$$-\mathcal{L} = -\mathcal{L}_{\varphi_1} + \chi(T) \left[1 - \cos\left(\arg \varphi \right) \right] , \tag{1.2}$$
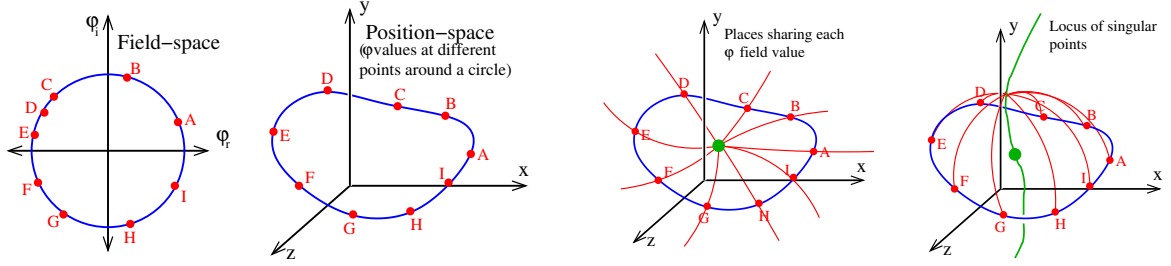
Figure 1. Illustration of the topological origin of strings. A series of points along the minimum of the potential in field-space (leftmost) may be mapped onto by a series of points along a loop in position-space (next-to-left). On a surface bounded by the coordinate-space loop, the set of points which map onto A, B, *etc.* each form a curve (third-from-left) which must meet at a singularity in θ_A. By considering a family of surfaces, there must be a locus of such singular points forming a string (rightmost).

with $f_a \sim 10^{11}$ GeV the axion decay constant (the vacuum value for the φ field) and $\chi(T)$ the temperature-dependent topological susceptibility of QCD. The decay constant f_a is a model parameter, and $\chi(T)$ is a calculable quantity in QCD, which is currently not well determined at high temperature [15, 16]. We will not address the problem of finding $\chi(T)$ here. Instead we focus on the topological consequences of a spontaneously broken global U(1) symmetry, which is also very weakly explicitly broken.

The φ field has heavy radial excitations with mass-squared $m_s^2 \equiv \lambda f_a^2$ and nearly-massless angular excitations with mass-squared $m_a^2 = \chi(T)/f_a^2$. At temperatures $T \ll f_a$ and length scales $r \gg f_a^{-1}$ we can treat φ as a classical field and treat the radial excitations as heavy, so the field is almost-everywhere on the "vacuum manifold" $\varphi^*\varphi = 2f_a^2$. Then we can write $\sqrt{2}\,\varphi = f_a e^{i\theta_A}$, with $\theta_A = \arg\varphi$ the "axion angle"; the potential energy is only very weakly dependent on the value of θ_A through the symmetry breaking term, which at high temperatures (roughly $T > 1.5$ GeV) can be ignored. The angle θ_A is only defined modulo 2π. It is possible for the field to leave the vacuum manifold along a linelike defect, with θ_A varying by 2π around any loop which circles the linelike defect in a positive sense (see figure 1).

Such a defect — essentially a vortex in the φ field — is called an axionic cosmic string, and it is topologically stable; no local changes to the value of φ can cause it to disappear. If PQ symmetry is restored in the early Universe, then θ_A starts out uncorrelated at widely separated points and will generically begin with a dense network of these strings (the Kibble mechanism for string production [17]). The strings evolve, straightening out, chopping off loops, and otherwise reducing their density, arriving at a scaling solution [18] where the length of string per unit volume scales with time t as t^{-2} up to logarithmic corrections (which we will discuss).

Let us analyze the structure of a string in a little more detail. Consider a straight string along the z axis; in polar (z, r, ϕ) coordinates the string equations of motion are solved by $\sqrt{2}\varphi = v(r)f_a e^{i\phi}$, with $v(r) \simeq 1$ for all $r^2 \gg 1/(\lambda f_a^2)$; so $\theta_A = \phi$ (up to a constant which we can remove by our choice of x-axis). The string's energy is dominated by the gradient energy due to the space variation of θ_A:

$$T = \frac{\text{Energy}}{\text{length}} = \int r\, dr\, d\phi \left(V(\varphi^*\varphi) + \frac{1}{2}\nabla\varphi^*\nabla\varphi \right) \tag{1.3}$$

$$\simeq \pi \int r\, dr \left(\frac{\partial_\phi \varphi^*}{r} \frac{\partial_\phi \varphi}{r} \right) \simeq \pi \int_{1/m_s}^{H^{-1}} r\, dr\, \frac{f_a^2}{r^2} = \pi f_a^2 \ln(m_s/H) \equiv \pi f_a^2 \kappa, \tag{1.4}$$

– 2 –

where the integral over r is cut off at small r by the scale where $v(r) \neq 1$ (the string core), and at large distances by the scale where the string is not alone in the Universe but its field is modified by other strings or effects, which we took to be the Hubble scale H^{-1}. We define $\kappa = \ln(m_s/H) = \ln(f_a\sqrt{\bar{\lambda}}/H)$ as the ratio of these scales; typically $f_a \sim 10^{11}$ GeV, while at the relevant temperature range $T \sim 1\,\text{GeV}$ the Hubble scale is $H \sim 10^{-18}$ GeV, so $\kappa \sim 70$ (unless λ is orders of magnitude smaller than 1).

This logarithm, κ, controls several aspects of the strings' dynamics. It controls the string tension, as we just saw. More relevant, while the string tension is $\pi\kappa f_a^2$, the string's interactions with the long-range φ field scale as f_a^2. Therefore the string's long-range interactions become less important, relative to the string evolution under tension, as κ gets larger. The long-range interactions are responsible for energy radiation from the strings, as well as for long-range, often attractive, interactions between strings. Since these effects tend to deplete and straighten out the string network, the large-κ theory will have denser, cuspier strings. Indeed, in the large κ limit the string behavior should go over to that of local (Nambu-Goto) strings [19], which are known to have far denser string networks than axionic networks with $\kappa \sim 6$.

In our first paper on this subject [20], we simulated string networks, with and without the potential-tilting term of eq. (1.2), in "field-only" classical lattice simulations where the string cores arose naturally from treating both radial and angular components of the φ field.[1] Therefore, the scales m_s and H both had to be resolved on the lattice, which restricts the ratio to be less than the number of points across the lattice N. Realistically $N \leq 2^{11}$ in 3D simulations and $N < 2^{16}$ in 2D, which limited us to studying the range $\kappa \leq 6$ in 3D and 8 in 2D. We followed the string evolution through the regime where the potential tilt, eq. (1.2), becomes important and even dominant. Domain walls develop and destroy the string network [25], leaving behind axionic fluctuations whose density we seek to determine. Over the κ range we could observe, we saw clearly that the density of strings depends strongly on κ. We also found that the behavior of the system in 3+1 dimensions, in terms of string density, energy density, and final axion number produced, is surprisingly similar to that in 2+1D, by which we mean 3+1D but with all fields constant along the z direction. Finally, we found that the axion production rate was a surprisingly weak function of κ. Indeed, over the range we studied, axion production actually decreased slightly as we raised κ.

Unfortunately, the physical value of $\kappa \sim 70$ is an order of magnitude larger than we could achieve with field-only methods. The density of strings is presumably much larger for $\kappa = 70$, as predicted by one-scale models [26]. And we know the string tension scales linearly with κ, as in eq. (1.4). It seems reasonable to expect that, as these denser networks of higher-energy strings decay into axionic excitations, the final axion number density will be higher than in the small-κ simulations (though we see no sign of this for the κ range we have been able to study). But to verify this suspicion, and really learn the axion production efficiency, we need to simulate axion production using this larger κ value. This paper will show how to do this in full detail in 2+1 dimensions, and will argue for how to extend the methodology to 3+1 dimensions. The basic idea of the simulations is to implement the angular component θ_A of the φ field on the lattice, while implementing string cores as additional explicit objects (not restricted to the lattice) which interact appropriately with the lattice θ_A field. Conceptually this is similar to the work of Dabholkar and Quashnock [19]; but their work was analytical and did not present an algorithmic implementation for the lattice. In the next section, we explain

---

[1]There have been other field-only classical field theory simulations [21–24], with similar results but with less dynamic range of κ values explored.

the method for the 2+1 dimensional problem, by taking advantage of a dual electromagnetic description. Section 3 presents the details of the lattice implementation. In section 4 we explore the numerical results. These lead us to expect that the physics of 2+1D and 3+1D become ever more different as the string cores get higher-tension. Therefore, while our results are suggestive, we cannot interpret them too literally for the interesting 3+1D case. We close by describing how our algorithm can be extended to 3+1 dimensions.

2 The dual electromagnetic picture

The basic idea of our method is the following. At large distances $r \sim H^{-1}$ or $r \sim m_a^{-1}$ the θ_A field displays complicated dynamics which we need to solve nonperturbatively, via lattice simulations. The field also contains topological defects. The cores of the defects involve very short scales, as we have already emphasized. But the physics of these string cores is actually very simple, and we understand it analytically. On short scales the string is very straight, and in its local rest-frame the θ_A field varies around the string with the angular ϕ-coordinate, up to corrections subleading in $m_a r$ or Hr.

It is a waste of effort to try to simulate the microscopic behavior of the string core by solving the field equations of motion. Instead we should "cut it out" from our lattice and "sew back in" an explicit object which reproduces the string core's behavior. The main challenge is to incorporate correctly the physics of how the string influences θ_A in its environment, and how the environment influences the string evolution. In this section we will show how to do that — for the 2+1 dimensional theory.

2.1 2+1D string defects as electromagnetic charges

Consider the axion model in 2 space dimensions. For ease of presentation we will explain the approach in flat, non-expanding space. It is straightforward to re-introduce Hubble drag and to work in terms of conformal time.[2] Except within a tiny distance $r \sim 1/m_s$ of a string core, the axion field is determined by θ_A alone; ignoring for now the symmetry-breaking potential term, its Lagrangian and equation of motion are

$$-\mathcal{L}_{\theta_A} = \frac{f_a^2}{2} \partial_\mu \theta_A \partial^\mu \theta_A \,, \qquad \partial_\mu \partial^\mu \theta_A = 0 \,. \tag{2.1}$$

A "string" defect in 2+1 dimensions is a point (monopole) defect, with $\nabla \theta_A$ diminishing as $1/r$ radiating out from the defect. This is the same falloff as the electric field of a charge in 2+1 dimensions. The potential between two strings also has the same $-\frac{q_1 q_2}{2\pi} \ln(r)$ form as in 2+1D electromagnetism. Indeed, there is actually a perfect analogy between the axion field and electromagnetism [27]. If we define

$$F_{\mu\nu} = -f_a \epsilon_{\mu\nu\alpha} \partial^\alpha \theta_A \tag{2.2}$$

with $E_i = F_{i0} = F^{0i}$ and $B = F_{12}$, so in components[3]

$$E_i = f_a \epsilon_{ij} \partial_j \theta_A \,, \qquad B = f_a \partial_t \theta_A \,, \tag{2.3}$$

---

[2]Axion number is set around $T \sim 1\text{GeV}$, when the universe is radiation dominated and the number of relativistic degrees of freedom g_* is nearly constant. The Hubble parameter is $H = \partial_t a_H / a_H = 1/2t_{\text{true}}$. Conformal time t_{conf}, henceforward just t, is $dt = dt_{\text{true}}/a_H$. The temperature scales as $T \propto t^{-1}$ and the metric scales as $g_{\mu\nu} \propto t^2 \eta_{\mu\nu}$. Therefore mass scales in these units grow with an extra t factor relative to the physical mass. Our sign conventions are that $\eta_{\mu\nu} = \text{Diag}\,[-1, +1, +1, +1]$ and $\epsilon_{0123} = 1 = -\epsilon^{0123}$.

[3]Recall that in 2+1 dimensions, the magnetic field is a pseudoscalar (corresponding to B_z in 3+1D).
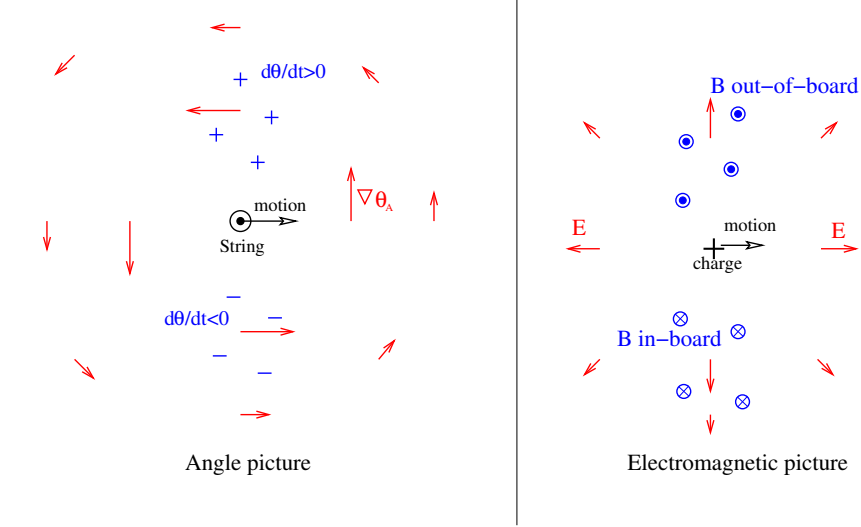
Figure 2. The dual pictures: a moving string in terms of angles (left) and in terms of electromagnetic fields (right).

then away from string cores these fields obey Maxwell's equations,

$$\partial_\mu F^{\nu\mu} = -f_a \epsilon^{\nu\mu\alpha} \partial_\mu \partial_\alpha \theta_A = 0 \,, \tag{2.4}$$

$$\epsilon_{\mu\nu\alpha} \partial^\alpha F^{\mu\nu} = -f_a \epsilon_{\mu\nu\alpha} \epsilon^{\mu\nu\beta} \partial^\alpha \partial_\beta \theta_A = 2 f_a \partial_\alpha \partial^\alpha \theta_A = 0 \,, \tag{2.5}$$

where the first holds by antisymmetry and the second requires the θ_A equation of motion.

The electric flux through a loop enclosing a positive-vorticity string is

$$\oint E_i \hat{n}_i dx \equiv \oint \epsilon_{ij} E_i dx_j = \oint f_a \partial_i \theta_A dx^i = 2\pi f_a \tag{2.6}$$

so the strings act as electric charges of charge $\pm 2\pi f_a$. Therefore axion field dynamics in 2+1D are equivalent to electrodynamics of particles with charge $\pm 2\pi f_a$. If we include all scales down to the string core scale, the electric charges' mass arises entirely from the field (self-)energy. But if we regulate the charges' self-energies at a scale r_0, then we can include the effect of very small string cores by giving the charges masses, $M = \pi f_a^2 \ln(m_s r_0)$, with m_s (again) the mass of the radial excitation or the inverse of the string core size. The electromagnetic duality for a string of positive winding number is illustrated in figure 2.

2.2 Regulation by smeared charges

The duality to 2+1 dimensional electromagnetism suggests that string cores can be treated as charged particles in a "particle-in-cell" approach [28]. To achieve a core size of $ae^{-\kappa}$, with a the lattice spacing and $\kappa \sim 70$, we could choose to make the charges have mass $M = \pi f_a^2 \kappa$. However, pointlike charges turn out to be problematic when interacting with a lattice electromagnetic field. The highest wave-number k modes of the lattice show Lorentz-violating unphysical behavior, and we must protect the point-charges from interacting with them through a form-factor, which is achieved by smearing the charge into a ball. Alternately, in the continuum we can view this as an explicit mechanism to regulate the UV contribution to the string's self-energy. The network dynamics will only be well represented on scales

larger than the radius of this ball. We will do our best to add in any physics which is disturbed by this ball, such as the interactions between strings when they get very close together. But since the final axion number is dominated by long-wavelength excitations, the regulation should not significantly impact our results for axion number generation.

We will show how to smear the charges in the continuum, and then find an implementation of the resulting equations on the lattice. The implementation we use will not be fully covariant; the ball's shape will not respond to Lorentz contraction and will respond instantly to changes in the charge's velocity, without retardation. These are minor problems in 2+1D if the charges are heavy, because they will then be nonrelativistic and their accelerations will be small.

To begin the implementation, we pick the charge distribution within the ball. Specifically, for a positive-charge string at position y we choose the charge density at x to be $\rho(x) = f_a g(|x - y|)$ with

$$\int g(x) \, d^2x = 2\pi \int r g(r) \, dr = 2\pi \,, \qquad g(r > r_0) = 0 \tag{2.7}$$

so the charge has compact support. We will also choose $g(r)$ to go continuously to zero as $r \to r_0$, so the charge density is continuous.[4] We will also introduce

$$f(r) \equiv \int_r^\infty r' g(r') \, dr' \tag{2.8}$$

which is the charge fraction lying outside radius r. It obeys $f(r > r_0) = 0$, $f(0) = 1$, and $df/dr = -r g(r)$.

For ease of presentation we will consider a single positive-charge string. The case of many strings just involves a summation and $\pm$ signs. The charge density modifies the Maxwell equations;

$$\partial_\mu F^{\nu\mu}(x) = J^\nu = f_a g(r) v^\nu \tag{2.9}$$

where $r_i = x_i - y_i$ is the vector from the charge's location y_i to the position of interest x_i and $v^\nu = (1, dy_i/dt) = (1, -dr_i/dt)$.

We need to find a modified set of θ_A field dynamics and a modified relation between $F_{\mu\nu}$ and θ_A under which eq. (2.9) is satisfied. There are two reasons to prefer to work in terms of θ_A. First, it is a more compact way of writing the physical degrees of freedom. Second, the symmetry-breaking potential is only known in terms of θ_A. We will modify eq. (2.2) by expressing it in terms of a "covariant" derivative of θ_A:

$$F^{\mu\nu} = -f_a \epsilon^{\mu\nu\alpha} D_\alpha \theta_A \,, \qquad D_\alpha \theta_A = \partial_\alpha \theta_A - A_\alpha \,. \tag{2.10}$$

We will discuss the physical interpretation of A_α in a moment. To ensure that Faraday's law still holds, we need to change the θ_A equation of motion:

$$0 = \epsilon_{\mu\nu\alpha} \partial^\alpha F^{\mu\nu} = 2 f_a \partial^\alpha D_\alpha \theta_A \,, \tag{2.11}$$

which are the equations of motion arising from the Lagrangian

$$\mathcal{L}_{\theta_A} = -\frac{f_a^2}{2} D_\mu \theta_A D^\mu \theta_A \,. \tag{2.12}$$

---

[4]In our numerical implementation we use $g(r) = 4(r_0^2 - r^2) r_0^{-4} \Theta(r_0 - r)$, so $f(r < r_0) = (1 - r^2/r_0^2)^2$.

Now we need to determine what choice for A_μ will ensure eq. (2.9) (Coulomb's and Ampere's laws) are satisfied. We have

$$\partial_\mu F^{\nu\mu} = -f_a \partial_\mu \epsilon^{\nu\mu\alpha} D_\alpha \theta_A = J^\nu \quad \Rightarrow \quad \epsilon^{\nu\mu\alpha} \partial_\mu A_\alpha = g(r) v^\nu. \tag{2.13}$$

The correct choice for A_μ to make this work is

$$A_i = -\epsilon_{ij} \frac{r_j}{r^2} f(r), \quad A_0 = \epsilon_{ij} \frac{v_i r_j}{r^2} f(r), \quad \text{or} \quad A_\mu = \epsilon_{\mu\nu\alpha} \frac{v^\nu r^\alpha}{r^2} f(r). \tag{2.14}$$

Note that $\epsilon_{\mu\nu\alpha} v^\nu r^\alpha / r^2$ is the derivative of the θ_A field around an isolated string $\theta_A^{\rm str}$. In other words, our choice for $A_\mu(x)$ is $A_\mu(x) = f(r)\partial_\mu \theta_A^{\rm str}(x)$. Therefore

$$\epsilon^{\nu\mu\alpha} \partial_\mu A_\alpha = \epsilon^{\nu\mu\alpha} \left(f(r)\partial_\mu \partial_\alpha \theta_A^{\rm str} + [\partial_\mu f(r)]\partial_\alpha \theta_A^{\rm str} \right). \tag{2.15}$$

The first term vanishes by antisymmetry/symmetry on the indices μ, α, while a little work and the relation $\partial_r f(r) = -rg(r)$ confirms that the second term reproduces eq. (2.13).

So the electromagnetic theory with smeared charges with smearing charge density $g(r)$ is equivalent to the theory of angles with $\partial_\mu \theta_A$ replaced by $D_\mu \theta_A = \partial_\mu \theta_A - A_\mu$ and A_μ given in eq. (2.14). The relation between the charge density $g(r)$ and the modifier function $f(r)$ is $f(r) = \int_r yg(y)\, dy$ or $f'(r) = -rg(r)$.

Now we turn to the string's motion. The total Lagrangian for the system should be $L = L_{\rm str} + \int d^3x\, \mathcal{L}_{\theta_A}$, with $L_{\rm str} = -M\sqrt{1-v^2}$ the standard Lagrangian for a relativistic massive point particle. Varying with respect to the string's position, one finds

$$\partial_t \left(\frac{Mv_i}{\sqrt{1-v^2}} \right) = F_i, \tag{2.16}$$

where the force arises from the dependence of $\mathcal{L}_{\theta_A}$ on the string's location. We find the expected Lorentz force law,

$$F_\mu = \int d^2x\, \rho(x)\, F_{\mu\nu}(x) v^\nu \tag{2.17}$$

with space component

$$F_i = \int d^2x\, \rho(x)\, (E_i + \epsilon_{ij} v_j B) = f_a^2 \int d^2x\, g(|x-y|) \left(\epsilon_{ij} D_j \theta_A + \epsilon_{ij} v_j D_t \theta_A \right). \tag{2.18}$$

The time component F_0 determines how fast the string and the field exchange energy. The form of eq. (2.17) ensures that $F^0 = v_i F_i$ as expected.

Let us pause to interpret these equations and in particular the role of A^μ. Far from a string, $A^\mu = 0$ and the equations of motion are as usual, $\partial_\mu \partial^\mu \theta_A = 0$. But near the center of the charge ball, where $f(r) \simeq 1$, the A_μ term cancels $\partial_\mu \theta_A$ provided that θ_A takes the form of the field near a string core, $\theta_A = \theta_A^{\rm str}$. So the energy is minimized by having $\theta_A \simeq \theta_A^{\rm str}$ in the interior. In particular, this forces a singularity onto θ_A at $r = 0$; the energy is only finite when θ_A possesses this singularity. In other words, when θ_A takes the cosmic-string form, the gradient energies associated with its spacetime variation at distances $r < r_0$ are cut off, and associated instead with the explicit string mass.

We need to choose M such that it incorporates the energy in the string from all scales $r < r_0$, where the $|D_i \theta_A|^2$ terms have been cut off. According to eq. (1.4), the string's energy (per length in 3+1D) is $f_a^2 \pi \int_{1/m_s}^{H^{-1}} dr/r$. The θ_A field gradients will capture the $f_a^2 \pi \int_{r_0}^{H^{-1}} dr/r$

part of this energy, so the mass M is required to capture the rest: $M = \pi f_a^2 \int_{1/m_s}^{r_0} dr/r = \pi f_a^2 \ln(r_0 m_s)$. We can think of this as a matching condition that the charge-ball treatment correctly captures the energy and inertia of the string.

When there are more than one string, each string responds to the θ_A field gradients caused by the other strings' presence, which induces inter-string interactions. Because the analogy to the electromagnetic theory is exact, these interactions are the same as the electromagnetic forces between charge balls. Since the theory is relativistic and has radiation fields, orbitally bound pairs of (oppositely-charged) strings tend to inspiral and annihilate. However, under the charge-ball description we have built, this inspiral will not proceed correctly. While strings at separation $R > 2r_0$ feel the usual Coulomb force between point charges, $\vec{F}_{\text{pt.chg}} = \pm 2\pi f_a^2 \vec{R}/R^2$ (in the nonrelativistic limit), when the charges get close together, the balls overlap and the strength of the interaction is reduced. It is important to re-introduce the missing Coulombic interaction, lost due to the overlap of the charge balls. Otherwise, the charges' inspiral and annihilation will not proceed. Define $h(R)$ as the fraction by which the Coulomb interaction of overlapping balls is smaller than that between point charges:

$$h(R) = \frac{|F_{\text{pt.chg}}| - |F_{\text{ball.chg}}|}{|F_{\text{pt.chg}}|} \,. \tag{2.19}$$

Then we should add an explicit force between nearby charges, of magnitude $h(R)F_{\text{pt.chg}}$. This procedure is not exact; it is only correct in the nonrelativistic limit. But this is actually a good approximation for large M/f_a^2, and in any case we only need to include the short-distance interactions roughly to ensure that the inspiral and annihilation proceeds.

When the strings pass nearer still, the replacement of point charges with balls also reduces their tendency to radiate, which requires an added radiation-reaction force. We discuss this radiation-reaction force in more detail in appendix A. With both forces included, we at least semi-quantitatively reproduce the physics of inspiral and annihilation.

Note however that if radiation is included by a radiation-reaction force rather than by explicit interactions with the θ_A field, the radiated energy and any associated axion number is lost to the system. This is a problem if our goal is to track the total energy in the θ_A field, but not if our goal is to determine the number of axions. The strings' mass-energy $2M$ is liberated by the inspiral process at small separation, with equal energy released in each equal logarithmic range of wave number. However, the axion number associated with an excitation of energy E and wave-number k is $n_{\text{ax}} = E/\omega_k \simeq E/k$, which becomes insignificant at large k. Therefore, from the point of view of tracking axion number in the 2+1D theory, it is not important to account for radiation after a binary pair of strings becomes tightly bound.

3 Lattice implementation

Now we present an implementation of these particle-in-cell equations on the lattice. The possibility of such an implementation is a key result of this paper. But readers who are not interested in such details can skip this section. We define the field θ_A on the sites of a 2D square lattice with spacing a, while the strings are taken to have continuous positions. Time must also be discretized, with spacing δa, $\delta \ll 1$. On each lattice link we define $D_i \theta_A$ as

$$D_i \theta_A(x) = \theta_A(x + a\hat{i}) - \theta_A(x) - A_i(x) \,, \tag{3.1}$$

and on the temporal link we define

$$D_0 \theta_A(x, t) = \theta_A(x, t + \delta a) - \theta_A(x, t) - A_0(x, t) \,. \tag{3.2}$$
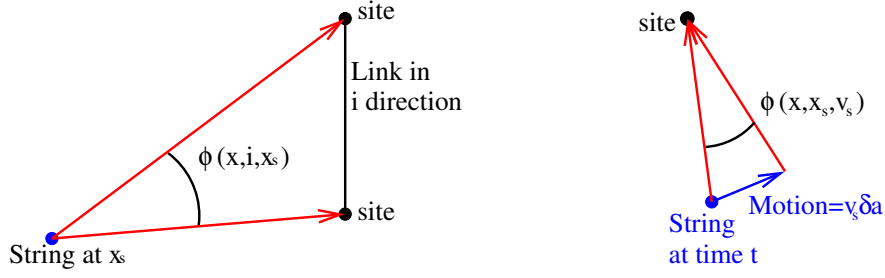
Figure 3. The angles $\phi(x, i, x_s)$, left, and $\phi(x, x_s, v_s)$, right.

The standard meaning for these derivatives would include additional factors of $1/a$ and $1/\delta a$. Note that $D_i\theta_A(x)$ really "lives" at $x + a\hat{i}/2$ halfway along the link, while $D_0\theta_A(x, t)$ really "lives" at time $(t + \delta a/2)$. Also, the $D_\mu\theta_A$ are only defined modulo 2π; we always take them[5] in the interval $[-\pi, \pi]$. The field update rule is

$$D_0\theta_A(x, t) = \frac{(t - \delta a/2)^2}{(t + \delta a/2)^2} D_0\theta_A(x, t - \delta a) \tag{3.3}$$

$$+ \frac{t^2\delta^2}{(t + \delta a/2)^2}\left[\frac{a^2\chi(T)}{f_a^2}\sin\theta_A + \sum_{i=1,2}\left(D_i\theta_A(x, t) - D_i\theta_A(x - a\hat{i}, t)\right)\right].$$

The factors of t^2, $(t \pm \delta a/2)^2$ incorporate Hubble expansion; the power 2 is because we are in conformal time in a radiation dominated universe.[6] We store $\theta_A(x, t)$ and $D_0\theta_A$ and perform this update by evaluating $D_i\theta_A$ on each link. The lattice definition of $A_i(x)$ is

$$A_i(x) = \sum_{\text{strings}} \pm f(|x + a\hat{i}/2 - x_s|)\phi(x, i, x_s),$$

$$\phi(x, i, x_s) = \text{atan}\frac{(x + a\hat{i} - x_s)_y}{(x + a\hat{i} - x_s)_x} - \text{atan}\frac{(x - x_s)_y}{(x - x_s)_x}. \tag{3.4}$$

That is, $\phi(x, i, x_s)$ is the angle subtended by the link from x to $x + a\hat{i}$ as seen by the string at point x_s, as illustrated in figure 3.

The angle $\phi(x, i, x_s)$ is the geometrical interpretation of $\int_x^{x+a\hat{i}}(-\epsilon_{ij}r_j/r^2)dx$ along the length of the link. Note that we evaluate $f(r)$ using the separation between the string's position x_s and the center of the link. In practice we find A_μ by performing a single loop over all strings with a nested loop over sites or links within a $2r_0 \times 2r_0$ box around each string. Therefore the algorithm scales linearly with system volume — though the numerical cost of finding A_μ scales as $(r_0/a)^2$ and dominates the numerical costs at early times when there are still many strings.

---

[5]Numerically, we implement both as integers; $\theta_A \in [0, 2^{29})$ are unsigned and $D_\mu\theta_A \in [-2^{28}, 2^{28})$ are signed, with bit masks used to enforce periodicity.

[6]Using conformal coordinates has two other effects. First, $\chi(T)/f_a^2 = m_a^2$ must be rescaled into conformal coordinates. If $\chi(T) \propto T^{-n}$ in physical units, then in conformal coordinates $a^2\chi(T)/f_a^2 \propto T^{-n-2} \propto t^{n+2}$. We return to this point at the start of section 4. Second, the string mass $M = \pi\kappa = \pi\ln(f_a r_0)$. Now f_a is fixed in physical units, but we keep r_0 fixed in comoving lattice units. Therefore M should slowly increase with time, $t\partial_t M = \pi$. The change over the physically interesting part of the evolution (roughly, $t = t_*$ to $t = 3t_*$) is small, and we have neglected this effect in this explorative study.

The value of $A_0(x,t)$ can be evaluated after we have determined how the string will move between t and $t + \delta a$. Defining the string velocity between times t and $(t + \delta a)$ as $v_s(t)$, the value of $A_0(x,t)$ is

$$A_0(x,t) = \sum_{\text{strings}} \pm f(x - x_s - \delta a v_s/2)\phi(x, x_s, v_s) \,,$$

$$\phi(x, x_s, v_s) = \operatorname{atan}\frac{(x - x_s - v_s \delta a)_y}{(x - x_s - v_s \delta a)_x} - \operatorname{atan}\frac{(x - x_s)_y}{(x - x_s)_x} \tag{3.5}$$

where ϕ is the angle change of the charge as it moves from x_s to $x_s + v_s\delta a$, as seen from the lattice site, also illustrated in figure 3. Again, this is the geometrical interpretation of $\int_t^{t+\delta a}(\epsilon_{ij}v_i r_j/r^2)dt$. Here x_s and v_s are both evaluated at t, so $g(r)$ uses the separation at time $t + \delta a/2$.

We will scale out the overall f_a^2 factor and write $M = \pi\kappa$ a pure number. The string's trajectory is determined by

$$x_s(t + \delta a) = x_s(t) + \delta a v_s(t) \,, \tag{3.6}$$

$$\frac{Mv_s(t)}{\sqrt{1 - v_s^2(t)}} = \left(\frac{t - \delta a/2}{t + \delta a/2}\right)^2 \frac{Mv_s(t - \delta a)}{\sqrt{1 - v_s^2(t - \delta a)}} + \left(\frac{t}{t + \delta a/2}\right)^2 \delta a(F_E(t) + F_B(t)) \,, \tag{3.7}$$

$$\pm F_{i,E}(t) = \sum_{x,j} \epsilon_{ij} g(|x + a\hat{j}/2 - x_s|)D_j\theta_A(x) \,, \tag{3.8}$$

$$\pm 2F_{i,B}(t) = \frac{(t - \delta a/2)^2}{\delta t^2} \sum_{x,j} \epsilon_{ij} v_{s,j}(t - \delta a)g(|x - x_s + v_s(t - \delta t)/2|)D_0\theta_A(x, t - \delta a)$$

$$+ \frac{(t + \delta a/2)^2}{\delta t^2} \sum_{x,j} \epsilon_{ij} v_{s,j}(t)g(|x - x_s - v_s(t)/2|)D_0\theta_A(x, t) \,. \tag{3.9}$$

The two components of the force are the electric force, from space gradients of θ_A, and the magnetic force, from its time derivatives. The one subtlety is that $v_{s,i}g(\dots)$ in the last line depends on the final velocity, which we don't know until we have computed it. The update is therefore implicit. We handle this by making an initial guess for $v_s(t)$ based on a linear trajectory, using it to evaluate the final magnetic force term, and iteratively re-substituting the determined v_s to recompute the magnetic force. The iteration converges by a factor of $\delta/M \sim 10^{-3}$ per repetition. $A_0(x,t)$ and therefore $\theta_A(x, t + \delta a)$ are only evaluated after $v_s(t)$ has been found.

To include the explicit forces between strings with separation $R < 2r_0$, we sort strings into boxes $2r_0$ on a side and search for nearby strings by comparing all string pairs in the same or neighboring (direct or diagonal) boxes. This approach keeps the algorithm linear in system volume. For each nearby string pair, we apply an inter-string force of $\pm 2\pi h(R)R_i/R^2$, with $h(R)$ defined in eq. (2.19). When strings pass even closer, with separation $\sim v_s r_0$, the radiative energy losses are not fully included, and we include a radiative reaction force, as motivated in appendix A. Lastly, we assume that any pair of strings which get closer than a distance $r_{\min} \ll a$ will annihilate, and rather than following their final inspiral we remove them from the simulation. When annihilating a pair of strings, we add a contribution to eq. (3.5) where $\phi(x, x_s, v_s)$ is the angle difference, as seen from the lattice site, between the two strings which will annihilate. This is the same as incorporating the shifts to the θ_A fields which would occur from sliding one string on top of the other before removing them from the

simulation. This prevents an unphysical "kick" to the fields when the strings annihilate and is especially important when the annihilating strings happen to be very close to a lattice site.

Our choice for initial condition is to draw $\theta_A \in [0, 2\pi]$ randomly at each lattice site, and then to apply a few steps of checkerboard nearest-neighbor smearing.[7] We identify vortices in the θ_A field using the algorithm presented in our previous paper [20], and place a string at the center of each square with such a vortex. Both $D_0\theta_A$ and v_s for all strings are initialized to zero, and this initial condition is assumed to apply at a time $t_i \geq 0$. The specifics of the initial conditions should not be too important since the network should converge towards a scaling solution; we discuss this more in appendix B.

It is possible for the θ_A field to have a vortex which is not associated with a string, or for a string to be far from any corresponding vortex or opposite-sign string. In each case this would reflect a misidentification of where strings should be based on the θ_A field; either a string is missing, or an extra string was included. That is, such errors occur when there is a failure in our initial conditions to make the strings and θ_A-field vortices coincide. This occurs, at a low rate, if we use 0 or 1 checkerboard smearings; it is exceedingly rare when we use more. We handle it by occasionally identifying these "missing" or "orphan" strings, and inserting or deleting them. All errors are caught at early times, and this operation should be interpreted as part of the initial condition setting algorithm.

4 Numerical results in 2+1 dimensions

It is necessary in any lattice study to ensure that the lattice regulation is not influencing the results. Therefore the first thing to check is that the (unphysical) parameters of the lattice setup do not influence results at sufficiently large scales and late times. The relevant parameters are δ, $r_{\min}$, r_0/a, and the specifics of our initial conditions choice. We leave the details of these checks to appendix B. Instead we check first what the scaling solution looks like, without the tilted potential but for different values of M. Then we solve for axion production in the case where eq. (1.2) is present and $\chi(T) \propto T^{-7}$, close to the value expected from instanton liquid models [29]. That means that the physical axion mass scales with conformal time as $m_{a,\text{phys}} \propto t^{7/2}$; but the conformal mass (the oscillation rate of the field in terms of conformal time) scales as one more power, $m_a t_* = (t/t_*)^{9/2}$ (which defines the scale t_* where the mass starts to play a role).

As we will see, there is a complication. For the case where the axion mass turns on with time, the string pairs cease annihilating and instead stay in tightly bound but surprisingly long-lived "atoms." In the end, we will have to make analytical estimates for the late-time axion production from these pairs, and cut them out from the simulation, to get the final axion number produced.

4.1 Scaling solution

First we look at string networks without tilting the potential, that is, keeping $m_a = 0$. Our goal is to see that the scaling solution exists, and to find the scaling of string density and velocity with M.

To do so we perform simulations at a range of masses from $M = 10$ to $M = 600$. As initial conditions we use 2 checkerboard smearing steps and an initial time t_i between 20 and

---

[7]One checkerboard step is to replace $\theta_A(x)$ on all "odd-checkerboard" sites with the average θ_A value of the 4 nearest neighbors, defined as the unit-circle projected position of the centroid of the neighbor-θ_A positions on the unit circle. The next checkerboard update changes the even-checkerboard sites.
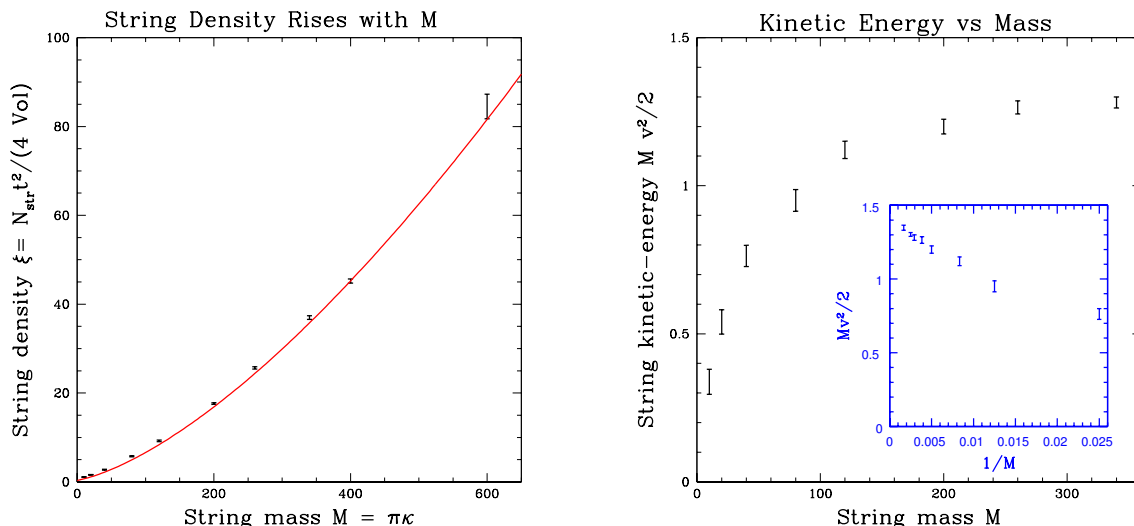
Figure 4. Density of strings (left) and mean kinetic energy in strings (right) as a function of the string mass M, at time $t = 1024$ in lattice units. The red line on the left shows $(M+15)^{3/2}$ behavior.

60, with larger values for larger M so that the string density starts near its scaling limit. We read out the string density at a final time $t = 1024a$ ($t = 2048a$ for the largest M value). Other parameters are set as described in appendix B.

Figure 4 shows the dependence of the string density and string velocity (plotted as $Mv^2/2$) on M. In our first paper [20] we make a parametric argument that Mv^2 should be nearly M independent, and that the string density should scale as M^1. We see that the first prediction is broadly correct. However, for the smallest M values, much of the string's energy resides in gradients in the θ_A field which are not included in the value of M. Therefore it is $(M + \pi \ln(r_{\rm sep}/r_0))v^2$, and not Mv^2, which should be approximately constant. Here $r_{\rm sep}$ is the mean inter-string separation. This explains why the smallest M values do not follow the expected trend. But for large M values, where the scaling argument should be more secure, the behavior is as expected.

On the other hand, the string density definitely does *not* scale linearly with the string mass M. Instead it rises as a larger power, roughly $M^{3/2}$. The red curve in the figure illustrates $(M+15)^{3/2}$ behavior, with $15 \sim \pi \ln(r_{\rm sep}/r_0)$. This is clearly a much better fit than a straight line. We believe that this difference is because the argument in [20] assumed that the most numerous strings are those which have not become bound into tight orbital pairs. It estimated the density of such strings based on the time scale for two strings to get close to each other, and then simply assumed that they will quickly annihilate. But we show in appendix A that this is not so; the time it takes a bound pair of strings to inspiral and annihilate is $t_{\rm inspiral} \sim RM^{3/2}$. Assuming $R \sim tM^{-1/2}$ as in the scaling solution in [20], the inspiral time is $\sim tM$, long compared to the system age. Therefore the inspiral process takes much longer than the process for strings to find each other, and most strings at any time are those which have bound off in pairs and are inspiraling, not strings "at large" as we assumed in [20]. This behavior is clear on visual inspection of the location of strings in a simulation: as an example, we plot the string locations for part of the volume of an $M = 400$ run at $t = 1024a$ in figure 5. Tightly bound string pairs obey a Virial relation, $Mv^2 = \pi$, as shown in the appendix. And indeed, in the inset of figure 4 it appears that $Mv^2/2$ asymptotes to ~ 1.4, somewhat below but in reasonable agreement with this relation.
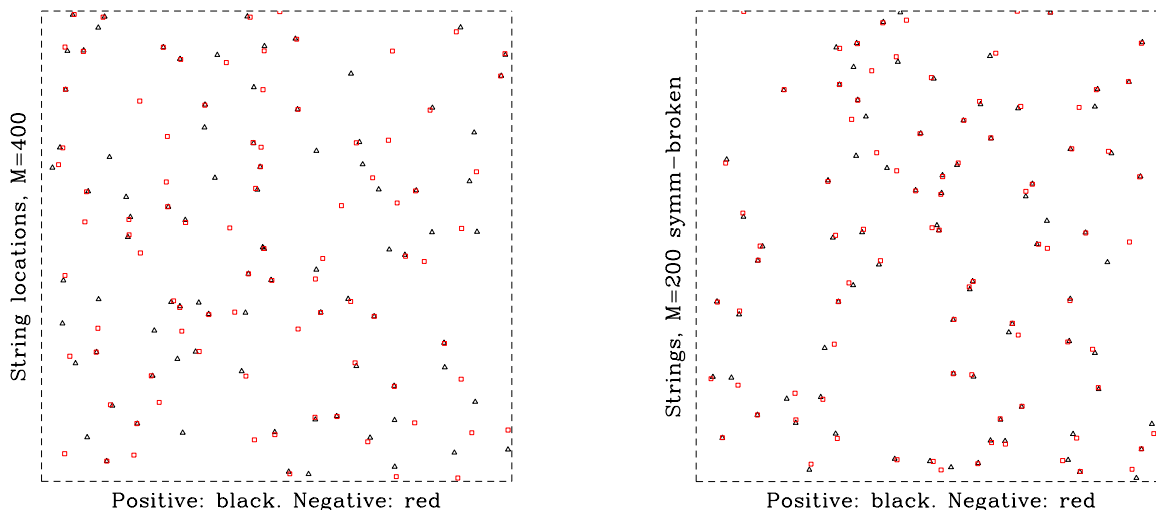
Figure 5. Location of positive (black triangles) and negative (red squares) strings in space: left, for an $M = 400$ simulation with no axion mass (untilted potential), and right, for an $M = 200$ simulation with a tilted potential at time $t = 3t_*$. On the left, most strings are in associated pairs; at right, they all are, and the pairs are tighter.

The situation here is loosely analogous to what we expect in 3+1 dimensions. Strings which have not bound off into pairs are analogous to long strings, and the tightly bound pairs are like string loops. For small M, radiation and inter-string attraction are important, and string loops decay rapidly via radiation — or pairs spiral in quickly in 2+1 dimensions. But for large M, radiation is inefficient, and loops can persist for a long time. Therefore the relative importance of loops (bound pairs in 2+1D) increases with increasing M.

4.2 Axion production

Next we turn to axion production. Following our previous work [20], we take $\chi(T)$ to vary with temperature as $\chi(T) \propto T^{-7}$, in which case the $\sin \theta_A$ term in eq. (3.3) should scale with conformal time as t^9. We define t_* as the time such that $m_a t_* = 1$, and we evaluate axion number at late time and match it to the adiabatic behavior under Hubble expansion (scaling out f_a factors):

$$n_{\mathrm{ax}} = \frac{1}{2} \int \frac{d^3 k}{(2\pi)^3} \left(\sqrt{k^2 + m_a^2} \langle \theta_A^2 \rangle + \frac{\langle (\partial_t \theta_A)^2 \rangle}{\sqrt{k^2 + m_a^2}} \right)$$
$$\simeq \frac{K t_*}{t^2} \quad \text{for } t \gg t_* . \tag{4.1}$$

As a baseline, the value of K for the case where θ_A is uniform and we average over the possible angle choices is $K = 16$. Our fields-only simulations implied $K \simeq 9$, valid in 2+1D for the small $\kappa \sim 8$ we could achieve. In 3+1D with $\kappa \sim 6$, fields-only simulations gave $K \simeq 8$.

It appears straightforward to determine K as a function of M in our 2+1D simulations. There is one problem, however. The axion number should be measured at late times when all strings have annihilated and the fluctuations in the θ_A field are perturbative. This is the condition that n_{ax} be an adiabatic invariant, which we rely on to relate the determined value to the value later in the history of the Universe. This works fine for small values of M.
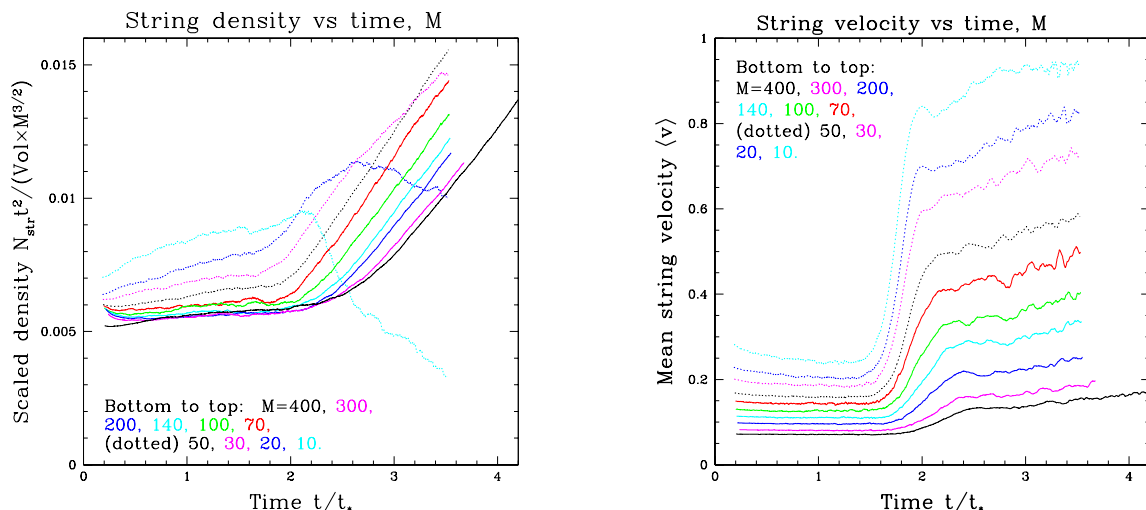
Figure 6. String density (left) and mean string velocity (right) as the effects of m_a and the associated domain walls come to be felt. The string velocity increases, and for small M the string density falls; but for large M the string density rises relative to the expected t^{-2} behavior which would occur in the absence of m_a (that is, if the potential did not tilt).

Indeed, in our fields-only study, we found that the strings annihilate away by around $t = 3t_*$. But for larger values of M which we can now study, such as the value $M \simeq \pi \ln(f_a/H) \sim 200$ which we argue is physically reasonable, the strings actually don't annihilate away, or at least they do so over a very long time scale. We illustrate this in figure 6, which shows the string density (left) and string velocity (right) as a function of t/t_*, for a number of choices of M. We have multiplied the string density by a factor of t^2 to account for its scaling behavior, and by a factor of $(M + 15)^{-3/2}$ to scale out the M-dependence found in the last subsection. The figure shows that, at a time around $t \simeq 1.8t_*$ (somewhat larger for larger M), the strings start to feel the added force from domain walls and pick up speed. This causes them to bind off into much tighter string pairs. For small M values, the strings then annihilate. But for large M, the density of strings actually falls more slowly than it would in the absence of a potential for θ_A. That is, tilting the potential so the strings attract each other more strongly actually *reduces* their tendency to annihilate. Therefore the curves in the figure, which are scaled by t^2 to compensate for the scaling behavior, rise. We show that the strings are in tight pairs in the right image in figure 5, which shows part of a simulation for $M = 200$ at $t = 3t_*$.

The tilting of the potential causes domain walls which draw the strings together and cause the increase in string velocity. But it also raises the minimum frequency of isolated axion oscillations. This creates a mismatch between the low orbital frequency of the string pair and the higher minimum oscillation frequency of radiated axions, which can prevent dipole radiation. Instead the orbital pair can only radiate at very high, and therefore inefficient, multipole number. For large values $M \sim 200$ which are relevant phenomenologically, we cannot carry out a simulation long enough for all of the string pairs to annihilate. Therefore we must find some procedure to estimate the axion number which will result when the string pairs eventually do annihilate.

Let us investigate the evolution of a bound string pair in this regime, neglecting radiation and scattering with any other axions present. We will also ignore the center of mass motion

of a string pair, which is smaller than the relative motion and which redshifts away. The potential between the strings is well approximated by

$$V(r) = 8m_a r - 2\pi E_1(mr) \tag{4.2}$$

with $8m_a$ the domain wall tension and $E_1(mr) = \int_r^\infty e^{-mx} dx/x$ the potential for a screened Coulomb interaction. We have verified this form numerically for static strings at fixed separation and $m_a r_0 \ll 1$. To simplify, we will neglect the Yukawa-like part of the potential and approximate this as $V(r) = 8m_a r$. Under a linear potential of this form, the Virial relation between potential and kinetic energies reads

$$\langle V(r) \rangle = 2\langle Mv^2 \rangle, \tag{4.3}$$

where v is the velocity of a string with respect to the center of mass (half the relative velocity), so Mv^2 is the total kinetic energy of the pair. The energy evolves adiabatically as the axion mass m_a rises and as Hubble damping depletes the kinetic energy. In our comoving coordinates,

$$\frac{dE}{dt} = \frac{dV}{dt} + \frac{d(Mv^2)}{dt} = \frac{dm_a}{m_a dt}\langle V \rangle - \frac{4}{t}\langle Mv^2 \rangle = \left(\frac{2}{3}\frac{dm_a}{m_a dt} - \frac{4}{3t}\right)E. \tag{4.4}$$

We used that radiation-era Hubble damping gives $dv/dt = -2v/t$ in conformal coordinates, and in the last step we used the Virial relation. For comparison, the energy in long-wavelength axionic fluctuations is scaling like

$$\frac{dE_{\text{ax.fluct}}}{dt} = \left(\frac{dm_a}{m_a dt} - \frac{2}{t}\right)E_{\text{ax.fluct}}, \tag{4.5}$$

where the first term is from the adiabatic growth of the axion mass and the second term is from Hubble drag. Using $dm_a/dt = 9m_a/2t$, we find that the energy in string pairs shrinks relative to already-produced axions as

$$\frac{E_{\text{pairs}}}{E_{\text{ax,fluct}}} \propto t^{-5/6}, \tag{4.6}$$

so the string pairs grow less important with time. Therefore, the longer it takes for them to radiate away their energy into axions, the smaller the produced axion number becomes.

We cannot follow the evolution past when $m_a a > 1$, and our description starts to break down when $m_a r_0 > 1$. We reach slightly larger times by reducing r_0 near the end of the simulation to keep $m_a r_0 \leq 1$, but we do not dare go beyond $r_0 = 2a$ for reasons discussed in the appendix. So we need some technique to estimate how much of the energy in the strings will convert into axion number. Our idea is to evolve the system as long as possible, and then to remove the strings and domain walls from the simulation in a way which leaves some of their energy behind, to capture the axion number which they would have produced. We have tried two approaches:

1. When $m_a a = 1/2$ we remove all strings from the simulation and replace values of θ_A close to π with smaller values as follows: for $\theta_A(x) \in [\pi/2, \pi]$ we apply $\theta_A \to \pi - \theta_A$, and for $\theta_A(x) \in [-\pi, -\pi/2]$ we apply $\theta_A \to -\pi - \theta_A$. This keeps θ_A continuous and does not change $(\nabla\theta_A)^2$, though it reduces the potential energy and destroys all topological objects (which is the goal). We then evolve the fields until $m_a a \geq 1$ so the further evolution is completely adiabatic, and measure axion number.
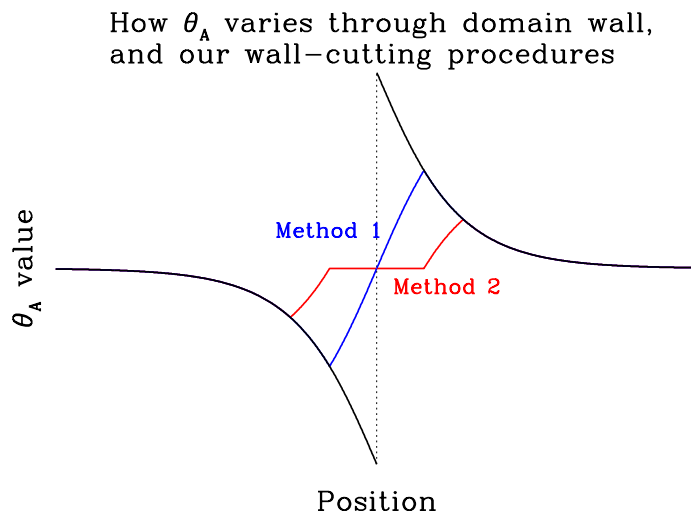
Figure 7. Illustration of how θ_A varies through a domain wall, and how each of our wall-chopping procedures work. The dotted line indicates periodicity, $\theta_A = -\pi$ and $\theta_A = \pi$ are equivalent.

2. We remove strings as above, but we remove the domain walls in a way which eliminates most of the energy they contain. We leave θ_A untouched in the range $[-\pi/4, \pi/4]$; in the range $[\pi/4, \pi/2]$ we apply $\theta_A \to \pi/2 - \theta_A$ (and similar for negative values), and wherever $\sin(\theta_A) < 0$ we replace θ_A with zero. This "cuts out" the cores of the domain walls in a way which does not introduce any discontinuities in the θ_A field. This approach is almost the same as removing the strings and domain walls entirely, on the assumption that they will not produce any axions.

The first approach converts most of the domain-wall energy into axions, while the second removes most of the domain-wall energy. They are illustrated in figure 7.

We can say something about which procedure is correct by seeing how the produced axion number depends on the time $t_{\rm cut}$ when the string-cutting is performed. We do this by varying the scale $t_{\rm cut}$ when the cutting is performed, holding everything else fixed. We improve the sensitivity by correlating the statistical errors, using the same random number seeds, so each $t_{\rm cut}$ choice is applied to the same network simulations. The results are shown in figure 8, where we have used $1/m_a(t_{\rm cut})t_*$ as the x-axis. This is roughly the inverse of the number of times the axion field oscillates and it indicates how adiabatic the axion oscillations have become. To get closer to 0 in this variable requires tightening the lattice spacing, linearly in this variable. We also plot what happens when we change the lattice spacing, or more precisely, when we vary t_*/a, keeping $m_a(t_{\rm cut})a$ fixed. This tests the same physics, but with added contamination of lattice-spacing (finite r_0/t_*) artifacts at the largest values. The axion-number estimates from the two string-cutting methods move towards each other as we postpone the cutting, albeit very slowly. It appears that the first/second method converge from above/below, in which case we can use them as upper and lower systematic-error limits on the actual axion production. The sensitivity to the string-cutting procedure is modest, representing $\sim 15\%$ of the axion production. But it will dominate over statistical errors and it limits our ability to extract a final axion number density.

Finally, we explore the M dependence of the axion number production. Figure 9 shows our results, which indicate a roughly linear rise with M in the axion production efficiency.
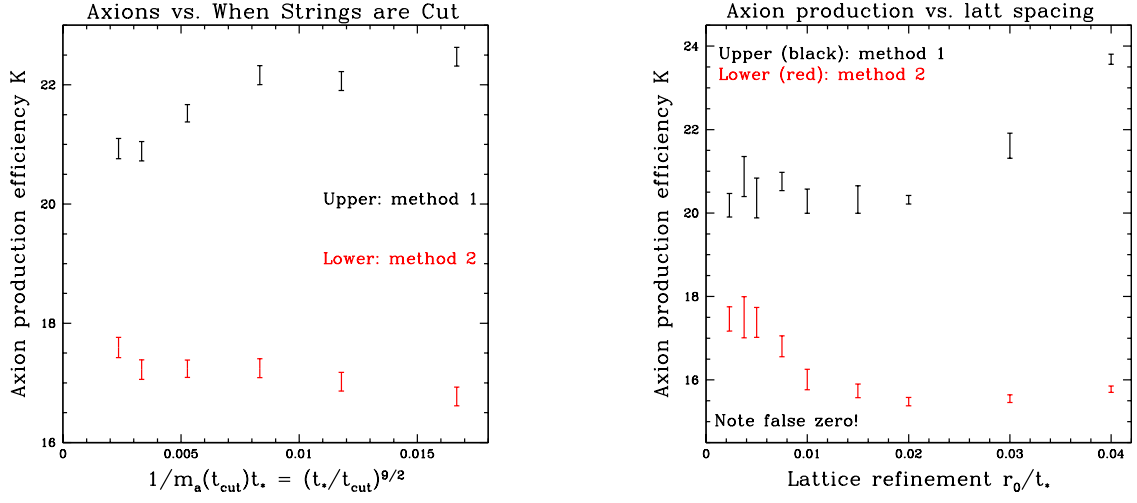
Figure 8. Axion production efficiency for $M = 200$ as a function of when the strings/walls are cut from the simulation. The upper (black) points are cutting procedure 1, the lower (red) points are procedure 2. Left: $t_*/a = 600$, varying the time t_{cut} when the strings are cut. Right: varying the lattice spacing t_*/a, always cutting at $m_a a = 1/2$.
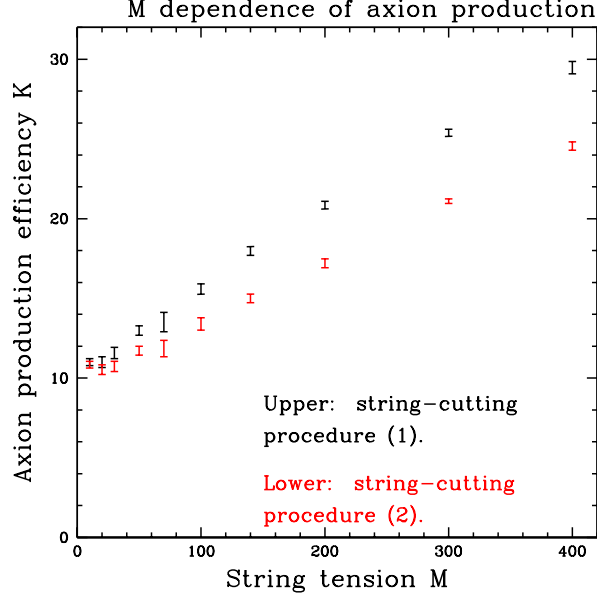

Figure 9. M dependence of axion number production efficiency K. Upper (lower) curves are the first (second) string-cutting procedure described in the text, and represent upper (lower) bounds on the systematic error, due to the longevity of orbiting string pairs.

For the physically relevant value $M \simeq 200$, we find $K \in [17, 20]$. The inclusion of large string tension has roughly doubled the axion production efficiency, relative to the results from fields-only simulations.

We postpone an interpretation of these results to the discussion section.

5 Extension to 3+1 dimensions

Suppose that we have an algorithm for evolving a Nambu-Goto string in 3+1 dimensions. Several such algorithms already exist [30–34]. We will require an algorithm which describes the string as a series of straight segments (or equivalently as a series of neighboring points, in which case we take the segments to be the line segments connecting these points). Our goal is to present an algorithm for implementing the interactions between these string segments and the axion field.

Consider a string with affine parameter σ. The location and velocity of the string are $y_i(\sigma, t)$ and $v_i(\sigma, t) = \partial_t y_i(\sigma, t)$ with $v^0 = 1$, $v_i \cdot y_i' = 0$, where $y_i' \equiv dy_i/d\sigma$. The latter is a gauge choice, that the velocity is at right angles to the string's extension. The action for the string and the θ_A field around it have been nicely discussed by Dabholkar and Quashnock [19]. The string core should obey a Nambu-Goto action plus an interaction with the θ_A field as follows. If we define the dual Kalb-Ramond [35, 36] field strength

$$H_{\mu\nu\alpha} = +f_a \epsilon_{\mu\nu\alpha\beta} \partial^\beta \theta_A \tag{5.1}$$

then H feels a current from the string,

$$\partial_\mu H^{\mu\alpha\beta} = j^{\alpha\beta}, \qquad j_{\mu\nu}(x) = -2\pi f_a \int d\sigma \delta^3(x - y(\sigma))(v_\mu y_\nu' - y_\mu' v_\nu), \tag{5.2}$$

with $y' = dy/d\sigma$. That is, just as in the 2+1 dimensional case, the string is responsible for a δ-function contribution to the curl in $\partial_\mu \theta_A$ which lies along the string's extension. We will again smear out the exact location of the Kalb-Ramond current,

$$j_{\mu\nu}(x) \rightarrow -\frac{f_a}{2} \int d\sigma g_3(x - y_i(\sigma))(v_\mu y_\nu' - y_\mu' v_\nu), \tag{5.3}$$

where $\int r^2 g_3(r) dr = 1$ so $\int d^3x \, g_3(x) = 4\pi$. Again we define $f_3(r) = \int_r^\infty g_3(r_1) r_1^2 dr_1$, which varies from 1 at small r to 0 for $r > r_0$, and then revert to the θ_A-field description. The derivative of the θ_A field should be modified to a covariant derivative

$$\mathcal{L}_{\theta_A} = -\frac{f_a^2}{2} D_\mu \theta_A D^\mu \theta_A, \qquad D_\mu \theta_A(x) = \partial_\mu \theta_A(x) - A_\mu(x), \tag{5.4}$$

$$A^\mu(x) = \int d\sigma \epsilon^{\mu\nu\alpha\beta} \frac{v_\nu r_\alpha y_\beta'}{2r^3} f_3(r) \tag{5.5}$$

with $r_i = x_i - y_i(\sigma)$. The force per unit σ acting on the string is

$$dF^\mu(y) = \frac{f_a^2}{2} \int d^3x \, g_3(r) \epsilon^{\mu\nu\alpha\beta} v_\nu y_\beta' D_\alpha \theta_A \tag{5.6}$$

which must be incorporated into the string's equation of motion. The usual equation of motion [37], defining

$$\varepsilon \equiv \mu \sqrt{\frac{(y')^2}{1 - (\partial_t y)^2}}, \tag{5.7}$$

is modified to

$$(H + \partial_t)(\varepsilon \partial_t y_i) = \partial_\sigma(\mu^2 \varepsilon^{-1} y_i') + dF_i \,. \tag{5.8}$$

Here $\mu = \pi f_a^2 \kappa$ is the string tension, which plays the role of M in the 2+1 dimensional theory. Again eq. (5.6) automatically ensures that $\partial_t \varepsilon = dF^0 = v_i dF_i$, and eq. (5.8) becomes

$$\partial_t^2 y_i = -H \partial_t y_i + \frac{\mu^2}{\varepsilon} \partial_\sigma(\varepsilon^{-1} y_i') + \frac{(\delta_{ij} - v_i v_j)}{\varepsilon} dF_j \,. \tag{5.9}$$

The $(\delta_{ij} - v_i v_j)$ term is the usual relativistic reduction of the acceleration along the direction of motion.

The special case in which θ_A is z-independent and all strings stretch strictly in the z-direction is equivalent to the 2+1D smeared-charge theory we previously presented, after identifying $g(r) = \frac{1}{2} \int dz g_3(\sqrt{r^2 + z^2})$.

The lattice implementation is as follows. The string must be considered as a series of short segments. The b'th segment has a basepoint y_b^i and an extent $s_b^i = y_{b+1}^i - y_b^i$, which plays the role of y'. Eq. (5.6) for a string segment is found by summing over all links close to a segment, using r in $g_3(r)$ as the distance from the center of the link to the center of the string segment and replacing y_b' with s_b. And

$$A^\mu(x) = \sum_b f_3(r) \frac{\phi(x, y_b, s_b, \mu)}{2} \,. \tag{5.10}$$

Here r is evaluated as the distance between the midpoint of the string segment and the midpoint of the lattice link for $\mu = i$, and as the distance from the lattice point to the middle of the string segment halfway between time t and $t + \delta a$ for the $\mu = 0$ case. And ϕ is a solid angle which is determined as follows. For $\mu = j$ it is the solid angle swept out by the string segment as one changes perspective by sliding along the lattice link. Equivalently, it is the solid angle, as seen from the base point x of the link, of the parallelogram with corners $\vec{y}_b$, $\vec{y}_{b+1}$, $\vec{y}_{b+1} - a\hat{j}$, and $\vec{y}_b - a\hat{j}$. For $\mu = 0$ it is the solid angle swept out by the motion of the string segment from time t to time $t + \delta a$, as seen from the lattice site.

It is clear that the lattice part of the update can be accomplished without much more difficulty than in the 2+1D case (though of course 3+1D simulations will be much more expensive numerically). It is not clear to us how best to implement eq. (5.9), but we believe that it should be possible to modify known Nambu-Goto algorithms to incorporate the force term. Nor is it clear to us, at present, whether it will be necessary to include explicit short-range inter-string interactions and radiation-reaction effects like the ones we used in the 2+1D theory. It is also necessary to keep track of when string segments intersect, since global strings are generally expected to intercommute [38].

6 Discussion

Axions present a well motivated dark matter candidate. With the additional assumption that PQ symmetry is restored in the early Universe, the model *should* be predictive in the sense that there should be a clean relation between the axion mass and the axion dark matter abundance.

The main stumbling block to finding this relation is the efficiency of axion production. This is hard to determine because it depends on the behavior of axionic strings, and the string dynamics are sensitive to the string tension, which varies logarithmically with the ratio

f_a/H. In nature (assuming axions exist) the ratio is $\sim 10^{30}$, while in fields-only numerical simulations it is $\leq 10^3$.

We have presented a new algorithm for solving this problem, by treating the string cores as additional explicit objects in a simulation of the axion field. We have presented, implemented, and studied this method in 2+1 dimensional space, and we have shown how it could be extended to 3+1 dimensions.

The axionic string networks in 2+1 dimensions are sensitive to the logarithm $\kappa \equiv \ln(f_a/H)$, with the density of strings rising roughly as $\kappa^{3/2}$ and the axion production increasing linearly with κ. Unfortunately, the physics of the strings which leads to this behavior does not look very much like the string network dynamics we would expect in 3+1 dimensions. The strings bind into long-lived orbital pairs, which are actually longer-lived and more numerous when the potential "tilts" than for the case with no explicit U(1) symmetry breaking. The longevity of these systems is partly because it is difficult to radiate massive axion excitations, and partly because they are nonrelativistic.

In 3+1 dimensions, we expect that increasing κ will lead to a denser string network which will produce more loops. Also, since strings radiate less efficiently, the loops can be longer-lived. But the motion of a string in 3+1 dimensions is generically relativistic, due to string tension effects. So 3+1D string loops should radiate much more effectively than the bound string pairs of the 2+1D system. As the explicit symmetry breaking becomes important, the long strings should strongly attract each other and annihilate or fragment into loops. So at, say, $t = 3t_*$, we expect 3+1D simulations to contain axions and small string loops.

It is possible that these loops will be long-lived, as their ability to radiate away their energy may be sufficiently suppressed because of the axion mass. So consider the case where they lose *no* energy to radiation of axions. In this case their energy density dilutes under Hubble expansion as a^{-3}, like matter. But the axions dilute like $a^{-3}m_a$, and $m_a \propto T^{-7/2} \propto a^{7/2}$ so long as the axion mass remains temperature dependent. Then the energy stored in string loops dilutes away relative to already-produced axions as $t^{-7/2}$, a much stronger power than eq. (4.6). Relative to our 2+1D simulations, any long-lived string structures should not play much of a role in 3+1 dimensions. Radiation from strings might still be important in 3+1D, even more important than in 2+1D, because of another difference. In 2+1D, almost all of a string's energy is always lost in the "final inspiral" to very short-wavelength axions with essentially no axion number. In 3+1D, cusps, bends, and waves along strings can turn string tension into axions, and a bigger fraction of the string network's energy may go into long-wavelength radiation.

For completeness we will update our results on the implied axion mass from [20], *assuming* that the axion production efficiency in 2+1D is the right one for the physical case of 3+1D. Taking the production efficiency to be $K = 19$ (between the upper and lower estimates for $M = 200$ in figure 9), and applying eq. (5.1)–(5.5) of [20], we find $T_* = 1.72\text{GeV}$, $f_a = 1.6 \times 10^{11}\text{GeV}$, and $m_a = 36\mu\text{eV}$. *However*, our discussion of the differences between the 2+1D and 3+1D cases gives us little confidence that the axion production efficiency in 2+1D is the same as in 3+1D. It is not even clear to us whether to expect the 3+1D axion production to be larger or smaller. What we have learned is that increasing the string tension really does increase axion production. But the above results can only serve as a crude guideline, not a real calculation.

It should be clear that 3+1 dimensional simulations, with strings as explicit objects which couple to θ_A fields, are needed. We have presented a nearly-complete algorithm for performing such simulations. The numerical effort to study the 3+1 dimensional problem

will be much ($\sim 10^3 \times$) larger than what was required here, but all of the results in this paper were generated in a few weeks on a single laptop, so 3+1D studies should be feasible.

Acknowledgments

A Charge inspiral

In the main text we need to know how efficiently a pair of vortices lose energy when they become bound to each other. This is equivalent to asking how an isolated, bound pair of electric charges in 2+1 dimensional electrodynamics radiates away energy. This is important both for understanding what to expect when charges get close together, and for adding explicit radiation when the charges are very close and we must incorporate radiation explicitly to account for its suppression due to a form-factor arising from the way we spread the charge into a ball. Unfortunately, there is no Larmor formula for radiated power in 2+1 dimensional electrodynamics, nor is there an Abraham-Lorentz expression for the radiation-reaction force. The reason is that Huygens' principle does not apply in 2+1 dimensions; the 4-vector field due to a charge is not determined by the 4-currents on the backwards light-cone of the field point, but by all 4-currents inside the light-cone.

We will first solve for the motion ignoring radiation and relativistic corrections. We will use this solution to determine the radiated power, and use it to determine how the charges must inspiral. For simplicity we will only solve for the case of a nearly-circular orbit. We find that the orbital velocity is constant and the charges follow an exponential spiral. Throughout, we scale out the irrelevant overall factors of f_a.

Consider two charges with $q = \pm 2\pi$ and charge separation R, so they are each $r = R/2$ away from the common center of mass. They each have mass M and an attractive force of strength $2\pi/R$ acts between them. Therefore, neglecting radiation reaction, they should follow circular orbits with velocity and frequency

$$\frac{\pi}{r} = F = \frac{Mv^2}{r} \quad \Rightarrow \quad v = \sqrt{\pi/M}, \qquad \omega = v/r = \sqrt{\pi/Mr}. \tag{A.1}$$

To find the associated radiation power, we consider the 2+1D theory as the same as the 3+1D theory with infinite line charges. We need to compute the far-field Liénard-Wiechert potential arising from the current-per-length of each charge. The charges have opposite current-per-length, each $2\pi v$, so the A_ϕ potential at a distance $d \gg 1/\omega$ from the charge pair is

$$A_\phi(d) = \frac{2 \times 2\pi v}{4\pi} \operatorname{Re} \int_{-\infty}^{\infty} \frac{d\ell}{\sqrt{d^2 + \ell^2}} e^{iv\sqrt{d^2+\ell^2}/r} e^{-i\omega t} \tag{A.2}$$

where ℓ is the distance along the (fictitious) 3'rd direction. The phase factor here is just the retarded phase $e^{-i\omega(t-D)}$ with the source distance $D = \sqrt{d^2 + \ell^2}$. Expanding in large d, we find

$$A_\phi(d) = v \operatorname{Re} \int_{-\infty}^{\infty} \frac{d\ell}{d} e^{-i\omega t + ivd/r} e^{\frac{iv\ell^2}{2dr}} = \frac{v}{d} \operatorname{Re} e^{i\cdots} \sqrt{\frac{2\pi dr}{v}} = \cos(\ldots)\sqrt{\frac{2\pi vr}{d}}. \tag{A.3}$$

The wave number is $k = \omega = v/r$ and $B = kA$. The power carried away by the wave is

$$P = 2\pi d \frac{E^2 + B^2}{2} = 2\pi d B^2 = \pi d k^2 A_{\phi,\text{peak}}^2 \qquad (A.4)$$

where the lost 2 is the average of the $\cos^2$. Substituting,

$$P = \frac{\pi d v^2}{r^2} \frac{2\pi v r}{d} = \frac{2\pi^2 v^3}{r} \, . \qquad (A.5)$$

This power is to be compared to the potential

$$V = \frac{q^2}{2\pi} \ln(2r) = 2\pi \ln(2r) \, . \qquad (A.6)$$

Here $2r = R$ is the separation of the charges. The value of r must evolve such that the power is the time derivative of the potential:

$$\frac{2\pi^2 v^3}{r} = \frac{dV}{dt} = \frac{2\pi}{r} \frac{dr}{dt} \, . \qquad (A.7)$$

We can then find $v_r = dr/dt$ and the time for the inspiral to complete:

$$\frac{dr}{dt} = -\pi v^3 \, , \qquad t_{\text{inspiral}} = \frac{r}{dr/dt} = \frac{r}{\pi v^3} = \frac{r M^{3/2}}{\pi^{5/2}} = \frac{R M^{3/2}}{2\pi^{5/2}} \, . \qquad (A.8)$$

The angle of the inspiral is fixed,

$$\sin\theta_{\text{inspiral}} \equiv \frac{-v_r}{v_\phi} = \frac{\pi v^3}{v} = \frac{\pi^2}{M} = \frac{\pi}{\kappa} \, . \qquad (A.9)$$

We have tested this description against the actual behavior of our code, for pairs of charges alone in a large box at separations $r > r_0$ but $r \ll Na$ the lattice size, and found good agreement.

Note that the inspiral process gives rise to an equal amount of energy in each logarithmic interval in frequency. Almost all of the charges' energy is released into extremely short wavelength fields, which carry very little axion number per unit energy. Therefore, once the charge separation has become smaller than the resolution scale of a simulation, it is safe to ignore the axion number produced by the subsequent inspiral, even though the energy release represents most of the energy present in the strings.

We have not solved for the case of a highly noncircular orbit, but we performed numerical experiments which suggest that the radiation-reaction force near the charges' closest passage is

$$F_{\text{rad.react.}} \simeq -\frac{\pi^3}{Mr}\hat{v} \, , \qquad (A.10)$$

which for the case of circular motion coincides with $F = -\pi^2 |v|\vec{v}/r$ as one would guess from eq. (A.5) (remembering that half the power is radiated from each charge). When the charges are far from closest approach, we find that the reactive force falls below the above estimate.

Generally the radiation-reaction force arises automatically from the coupling between the charges and the electromagnetic (θ_A) field. But in our lattice implementation we replace point charges with finite-sized charge balls. Any radiation with wavelength satisfying $kr_0 \leq 1$

is suppressed, since the current Qv is replaced by $v \int_y \rho(y) e^{i\vec{k}\cdot\vec{y}}$. Phase cancellation in this integral results in a form-factor suppressing the coupling to the radiative part of the θ_A field. Therefore we need to add a radiation-reactive force explicitly whenever the charges get so close that this effect suppresses their radiation. Failing to do so results in charges which stop inspiraling once they get sufficiently close. It is not necessary to include this effect with high precision, since it primarily affects strings which are about to annihilate; but we should include it to ensure that the annihilation really occurs. We do so by applying a reactive force equal to eq. (A.10) times $f(2vR/r_0)$, a crude estimate of the squared form factor. We could estimate the form-factor more accurately, but we have not done so because eq. (A.10) is already only an estimate.

The efficiency of radiation changes fundamentally if the axion mass is turned on. In this case, for an axion mass m_a, the radiation is suppressed whenever $\omega < m_a$, which for a circular orbit is when $r < v/m_a$ or $m_a r < v$. This is different from $m_a r < 1$, the criterion that the potential is significantly changed from the log form. For large M, radiation is suppressed even for charges far too close together for any "domain wall"-like behavior in their interaction energy. We have not found a good way to compute the radiated power in this case, but numerical experiments show that the suppression is severe and radiative energy loss essentially does not happen. We believe that this is a peculiarity of the 2+1D approximation which should be much less severe in 3+1D, where the string velocities will always be relativistic.

B   Checks and tests

Our numerical implementation contains several parameters, such as δ, r_0/a, $r_{\min}$, and the initial time t_i and amount of smearing used in the initial conditions. We have to ensure that there is some range for each parameter where we get continuum-like behavior, and determine at what time scale we achieve the scaling solution for the defect network. Our goal is results for the final axion number produced with few-percent systematic sensitivity to our implementation.

Let us start with δ and $r_{\min}$, the temporal step and the separation at which strings are taken to annihilate. Physically we want the limit where both go to zero, but numerically this is impractical. The bare minimum value for δ is set by the smaller of the Courant condition for the lattice field update, $\delta^2 < 1/2$, and the Courant condition[8] for the last steps of the inspiral of annihilating strings, $\delta^2 < M r_{\min}^2/\pi$. Also, our radiation-reaction method ceases to be energy-reducing when the separation approaches $r_{\min}$ unless $\delta^2 < M r_{\min}^2/(2\pi)$. It is less clear what the requirements on $r_{\min}$ are. The larger the value of $r_{\min}$, the more violent the process of removing two strings becomes; we also lose some radiation from the final inspiral if $r_{\min} > v r_0$.

We investigate $r_{\min}$ first. We fix $\delta = 1/20$ to be small, and consider $M = 200$ (corresponding to $\kappa = 64$, around the physical value), 10 passes of checkerboard field smearing in the initial conditions, $t_i = 0$, and $r_0 = 4a$, which we will later see is more than sufficient. We then consider the density of strings and the energy components in the θ_A field (without any tilt to the potential) for several values of $r_{\min}$.

---

[8]By the Courant condition we mean the δ-value beyond which some lattice mode or some pairing of strings will undergo oscillatory growth rather than stable evolution. Violating the condition for strings makes it difficult or impossible for pairs to annihilate; violating it for the fields leads to exponentially growing energy and fluctuations.
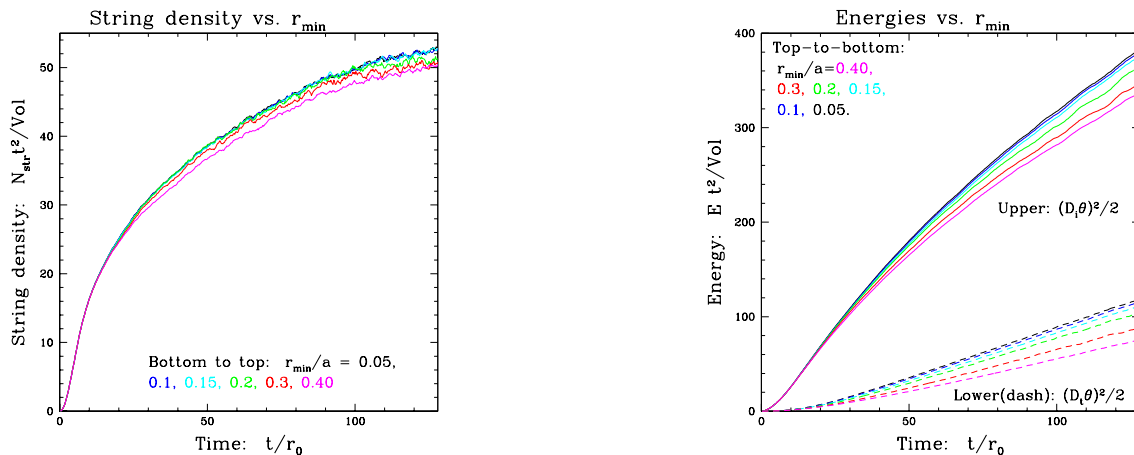
Figure 10. The dependence of vortex number (left) and scaled energy densities (right) on the cutoff separation where strings are taken to annihilate. The largest values show clear deviation, but for $r_{\min} = 0.15a$ and smaller the differences are negligible.

The results are shown in figure 10. We used the same random number seed for each $r_{\min}$ value, so the fluctuations in different curves are highly correlated and it is easier to see small differences over statistical noise. We plot the number of vortices in the θ_A field, rather than the number of strings, because once the strings get closer than $\sim a/2$ the associated vortices disappear, but different $r_{\min}$ values will consider the string pair to still exist for different lengths of time as they inspiral. Therefore the number of vortices avoids a trivial reason for the string counts to differ. We also compare the energy content in $(D_i\theta_A)^2$ (gradient energy) and $(D_0\theta_A)^2$ (kinetic energy). It is clear from the figure that too large a value of $r_{\min}$ causes strings to annihilate too soon, lowering the string density and also reducing the amount of field energy radiated before the strings annihilate. On the other hand, smaller values clearly approach a good limit. We will use $r_{\min} = 0.1$, since smaller values increase numerical cost without any clear benefit.

Fixing to $r_{\min} = 0.1$, we now consider δ, the temporal spacing. The results are shown in figure 11. Except for the coarsest temporal spacings, the value of δ is strikingly unimportant. This is good, as numerical cost scales as $1/\delta$. We conservatively choose $\delta = 1/6$ for all other studies, which should keep time-step errors below 1%.

Next consider the string core radius r_0. For r_0/a too small the strings do not have a smooth interaction with the lattice θ_A fields. The gradient energy associated with a string will have a short-distance contribution which is not translation-invariant, but depends on where the string sits with respect to the lattice. We can investigate this directly by considering lattices with two strings exactly halfway across the lattice from each other. We move around their exact location with respect to the lattice sites, evolving the lattice fields dissipatively to find the minimal-energy configuration for a given string location. The result is shown in figure 12, which shows how the energy varies as the string is moved along a path through the lattice. Values $r_0/a \sim 1$ show strong position dependence, which can interfere with the string's dynamics. In the units of the plot, a typical string kinetic energy is 2; so the energy variation through the lattice can trap slower-moving strings so they stick near the center of a lattice cell, rather than moving smoothly. For larger values $r_0 \geq 3$, the energy is a very weak function of the exact location on the lattice. For $r_0 = 4a$ the variation is invisible in the figure. For $r_0 = 2a$ it is accidentally small for this path.
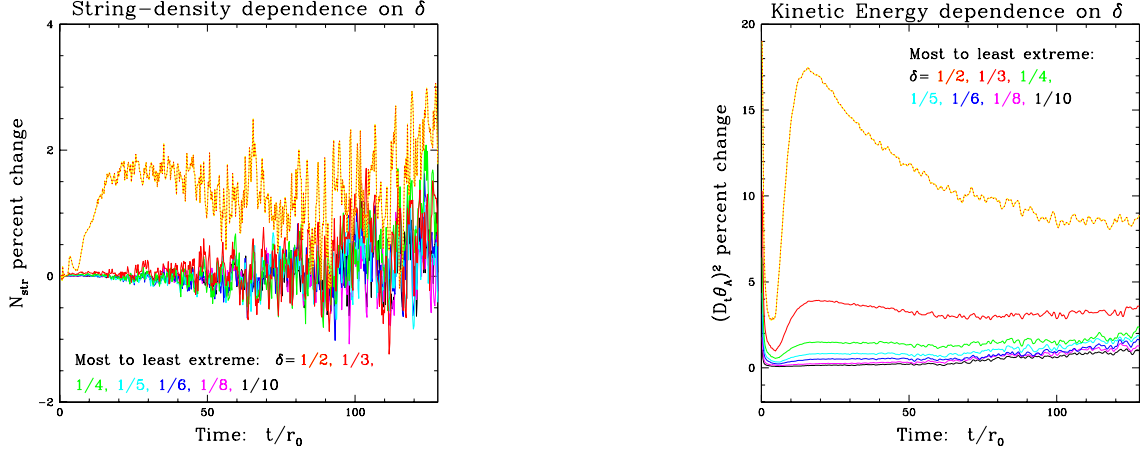
– 24 –

Figure 11. The dependence of string number (left) and scaled kinetic energy density (right) on the temporal spacing δ, shown as a percent change for identical initial conditions between the results with a given δ and the results with $\delta = 1/20$. Both are within 1% for $\delta = 1/6$ or smaller. Gradient energy shows less sensitivity than kinetic energy.
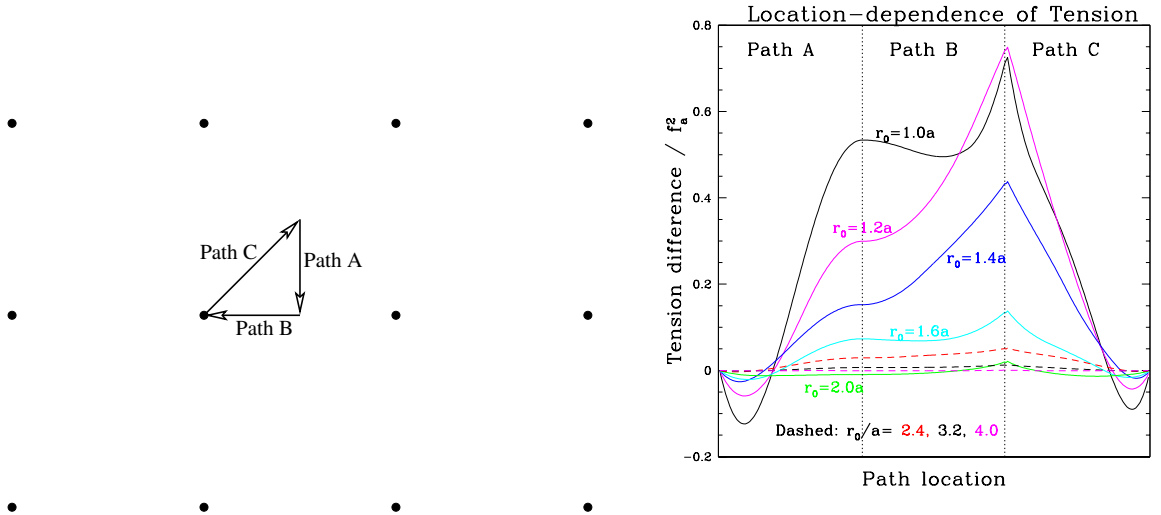

Figure 12. Left: a path through a lattice cell, in three steps. Right: how the string tension (the energy in the θ_A field gradients) varies as the string is moved along the path, for several values of the charge-smearing parameter r_0. Small values $r_0 < 1.6a$ give rise to strong position dependence in the string's energy.

As another probe of the impact of r_0, we evolve a lattice with only two strings of opposite charge, initially placed in a circular or elliptical orbit. This is a nice example of how orbital inspiral occurs, and a test of our short-distance force and radiation additions. It also lets us see how r_0 affects string dynamics. Figure 13 shows the coordinate-space track of one from a pair of inspiraling strings, evolved using several values of r_0. The figure shows that, for the smallest choice of $r_0 = 2a$, the charges interact with the lattice in a way which occasionally, abruptly, gives the system a net center-of-mass motion. This is clearly an artifact. Based on the figure, we consider $r_0 = 3a$ to be the minimal acceptable value. Since the numerical cost
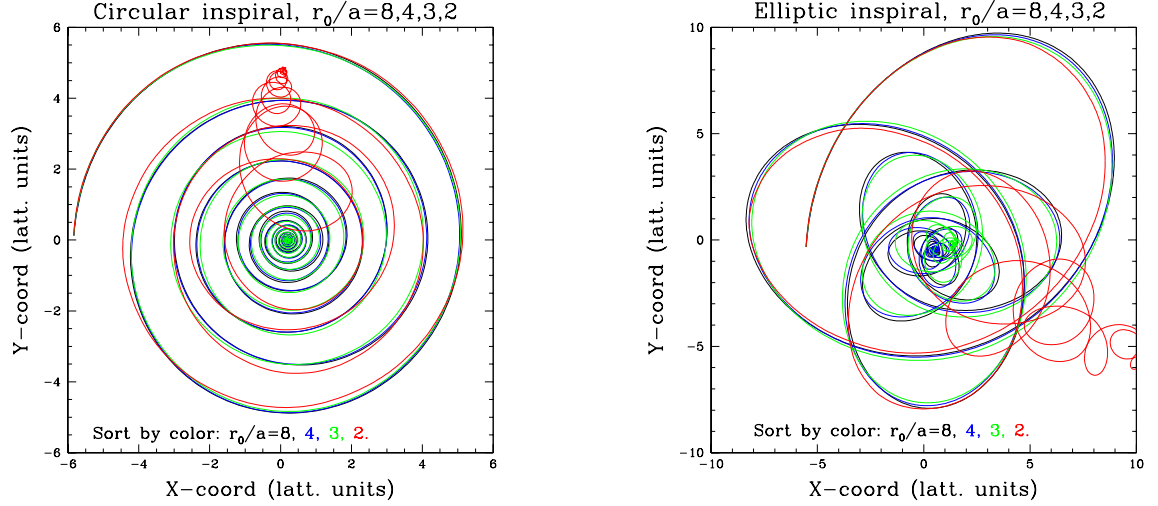
Figure 13. The path of one from a pair of orbiting, inspiraling strings, initially in a circular orbit (left) or an elliptical orbit (right). The different curves are for different choices of r_0, the charge-smearing radius. The values $r_0/a = 8$ (black), 4 (blue), and 3 (green) are in good agreement; however, for 2 (red) the charges bounce off of inhomogeneities in their potential with respect to lattice position, and the center of mass of the system takes on a net motion.
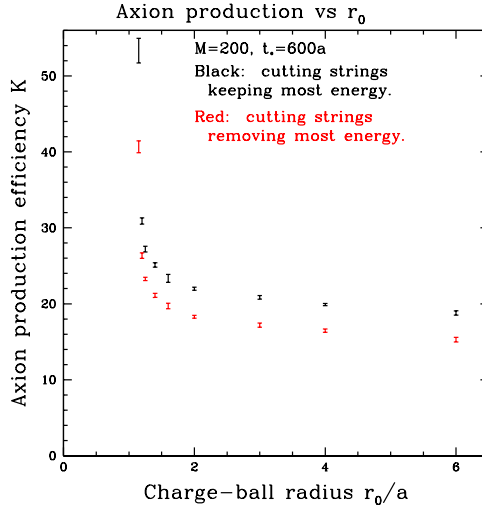

Figure 14. Dependence of axion production on r_0 choice. For small r_0 the strings get stuck and are overdense, and axion production is large. For $r_0 > 2$ there is a plateau, though the production falls slowly with increasing r_0.

to update the strings rises as r_0^2 and since larger values make it more difficult to achieve the small lattice-spacing limit, we will fix to this value in the following. The figure also illustrates that elliptical orbits rapidly precess, which is expected for a $1/r$ force law or $\ln(1/r)$ potential.

As another cross-check on the role of r_0, we also compute the axion number produced, for the $M = 200$ case, as a function of the r_0 value chosen. The result is plotted in figure 14. The procedure is as described in the main text, and as in the main text, we try two different
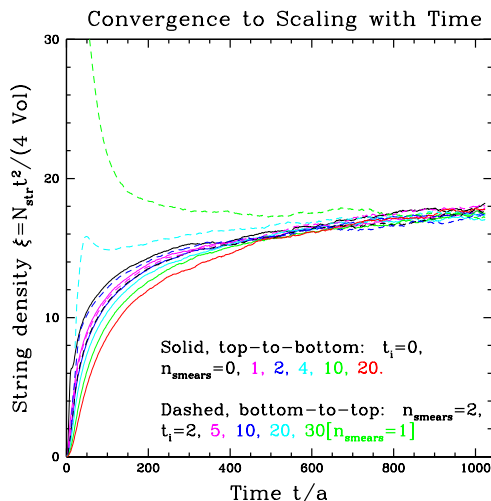
Figure 15. Dependence of scaled string density on the initial string density, determined by the number of smearing steps and the initial time t_i.

ways of addressing the strings which persist until late in the simulation: removing them but leaving most of the energy in the domain walls connecting them, or removing them and removing most energy in the domain walls. These are indicated with black and red points respectively. The figure shows that, below $r_0 = 2a$, the axion production rises steeply. For larger values it falls gradually with increasing r_0. Presumably this arises from effects where the charged balls are not much smaller than the scale of structure, or because large charged balls do not feel the right force strength when the domain walls become thin. If we make a linear extrapolation of the $r_0 \geq 3a$ data to $r_0 = 0$, we find about a 10% increase in the axion production efficiency K. We will treat this as a systematic error in the main text.

Finally, there is the amount of smearing we perform initially, which sets the initial density of strings, and the starting time t_i. These parameters can only affect how quickly the network approaches scaling; at sufficiently late times we should converge onto the same statistical ensemble of networks, possibly modulo short-range axionic fluctuations which carry little axion number. To study this issue we performed a series of simulations of string networks, using $t_i = 0$ with various numbers of initial checkerboard smearings and using 2 initial checkerboard steps with various values of t_i.

Figure 15 shows how the string density, scaled by a factor of $t^2/4$ to coincide with the scaling density ξ as defined in the literature,[9] depends on the number of smearing steps and on the initial time t_i. If $t_i = 0$ then the initial density is too low for any amount of smearing, including zero. But with an appropriate choice of t_i, we can reach the scaling solution rather quickly. In every case the scaling solution is reached by the end of the simulation; the final curves differ from each other by roughly the statistical errorbars (not shown for clarity), and we have checked that the string density does not change significantly if we continue the simulation to a larger time.

---

[9]ξ is defined as the string energy density, scaled by the string tension and the system age to form a dimensionless quantity. The factor of 4 is because it is conventional to use time and not confrmal time; in the radiation era there is a factor of 2 in the inter-relation. Since our strings are nonrelativistic, the number of strings is essentially the same as the string energy divided by the tension.

References

[1] R.D. Peccei and H.R. Quinn, *CP conservation in the presence of instantons*, *Phys. Rev. Lett.* **38** (1977) 1440 [INSPIRE].

[2] R.D. Peccei and H.R. Quinn, *Constraints imposed by CP conservation in the presence of instantons*, *Phys. Rev.* **D 16** (1977) 1791 [INSPIRE].

[3] S. Weinberg, *A new light boson?*, *Phys. Rev. Lett.* **40** (1978) 223 [INSPIRE].

[4] F. Wilczek, *Problem of strong p and t invariance in the presence of instantons*, *Phys. Rev. Lett.* **40** (1978) 279 [INSPIRE].

[5] G. 't Hooft, *Computation of the quantum effects due to a four-dimensional pseudoparticle*, *Phys. Rev.* **D 14** (1976) 3432 [*Erratum ibid.* **D 18** (1978) 2199] [INSPIRE].

[6] R. Jackiw and C. Rebbi, *Vacuum periodicity in a Yang-Mills quantum theory*, *Phys. Rev. Lett.* **37** (1976) 172 [INSPIRE].

[7] C.G. Callan Jr., R.F. Dashen and D.J. Gross, *Instantons as a bridge between weak and strong coupling in QCD*, *Phys. Rev.* **D 20** (1979) 3279 [INSPIRE].

[8] J. Preskill, M.B. Wise and F. Wilczek, *Cosmology of the invisible axion*, *Phys. Lett.* **B 120** (1983) 127 [INSPIRE].

[9] L.F. Abbott and P. Sikivie, *A cosmological bound on the invisible axion*, *Phys. Lett.* **B 120** (1983) 133 [INSPIRE].

[10] M. Dine and W. Fischler, *The not so harmless axion*, *Phys. Lett.* **B 120** (1983) 137 [INSPIRE].

[11] R.L. Davis, *Cosmic axions from cosmic strings*, *Phys. Lett.* **B 180** (1986) 225 [INSPIRE].

[12] P. Sikivie, *Experimental tests of the invisible axion*, *Phys. Rev. Lett.* **51** (1983) 1415 [*Erratum ibid.* **52** (1984) 695] [INSPIRE].

[13] R. Bradley et al., *Microwave cavity searches for dark-matter axions*, *Rev. Mod. Phys.* **75** (2003) 777 [INSPIRE].

[14] ADMX collaboration, S.J. Asztalos et al., *A SQUID-based microwave cavity search for dark-matter axions*, *Phys. Rev. Lett.* **104** (2010) 041301 [arXiv:0910.5914] [INSPIRE].

[15] S. Borsányi et al., *Axion cosmology, lattice QCD and the dilute instanton gas*, *Phys. Lett.* **B 752** (2016) 175 [arXiv:1508.06917] [INSPIRE].

[16] G. Grilli di Cortona, E. Hardy, J.P. Vega and G. Villadoro, *The QCD axion, precisely*, *JHEP* **01** (2016) 034 [arXiv:1511.02867] [INSPIRE].

[17] T.W.B. Kibble, *Topology of cosmic domains and strings*, *J. Phys.* **A 9** (1976) 1387 [INSPIRE].

[18] A. Albrecht and N. Turok, *Evolution of cosmic strings*, *Phys. Rev. Lett.* **54** (1985) 1868 [INSPIRE].

[19] A. Dabholkar and J.M. Quashnock, *Pinning down the axion*, *Nucl. Phys.* **B 333** (1990) 815 [INSPIRE].

[20] L. Fleury and G.D. Moore, *Axion dark matter: strings and their cores*, *JCAP* **01** (2016) 004 [arXiv:1509.00026] [INSPIRE].

[21] M. Yamaguchi, M. Kawasaki and J. Yokoyama, *Evolution of axionic strings and spectrum of axions radiated from them*, *Phys. Rev. Lett.* **82** (1999) 4578 [hep-ph/9811311] [INSPIRE].

[22] M. Yamaguchi, *Scaling property of the global string in the radiation dominated universe*, *Phys. Rev.* **D 60** (1999) 103511 [hep-ph/9907506] [INSPIRE].

[23] T. Hiramatsu, M. Kawasaki, T. Sekiguchi, M. Yamaguchi and J. Yokoyama, *Improved estimation of radiated axions from cosmological axionic strings*, *Phys. Rev.* **D 83** (2011) 123531 [arXiv:1012.5502] [INSPIRE].

[24] T. Hiramatsu, M. Kawasaki, K. Saikawa and T. Sekiguchi, *Production of dark matter axions from collapse of string-wall systems*, *Phys. Rev.* **D 85** (2012) 105020 [*Erratum ibid.* **D 86** (2012) 089902] [`arXiv:1202.5851`] [ɪɴSPIRE].

[25] A. Vilenkin and A.E. Everett, *Cosmic strings and domain walls in models with Goldstone and pseudo-Goldstone bosons*, *Phys. Rev. Lett.* **48** (1982) 1867 [ɪɴSPIRE].

[26] C.J. A.P. Martins and E.P.S. Shellard, *Extending the velocity dependent one scale string evolution model*, *Phys. Rev.* **D 65** (2002) 043514 [`hep-ph/0003298`] [ɪɴSPIRE].

[27] M.W. Hecht and T.A. DeGrand, *Radiation patterns from vortex-antivortex annihilation*, *Phys. Rev.* **D 42** (1990) 519 [ɪɴSPIRE].

[28] R. Hockney and J. Eastwood, *Computer simulation using particles*, Taylor & Francis, U.S.A. (1988).

[29] O. Wantz and E.P.S. Shellard, *The topological susceptibility from grand canonical simulations in the interacting instanton liquid model: chiral phase transition and axion mass*, *Nucl. Phys.* **B 829** (2010) 110 [`arXiv:0908.0324`] [ɪɴSPIRE].

[30] A. Albrecht and N. Turok, *Evolution of cosmic string networks*, *Phys. Rev.* **D 40** (1989) 973 [ɪɴSPIRE].

[31] D.P. Bennett and F.R. Bouchet, *High resolution simulations of cosmic string evolution. 1. Network evolution*, *Phys. Rev.* **D 41** (1990) 2408 [ɪɴSPIRE].

[32] B. Allen and E.P.S. Shellard, *Cosmic string evolution: a numerical simulation*, *Phys. Rev. Lett.* **64** (1990) 119 [ɪɴSPIRE].

[33] V. Vanchurin, K. Olum and A. Vilenkin, *Cosmic string scaling in flat space*, *Phys. Rev.* **D 72** (2005) 063514 [`gr-qc/0501040`] [ɪɴSPIRE].

[34] K.D. Olum and V. Vanchurin, *Cosmic string loops in the expanding universe*, *Phys. Rev.* **D 75** (2007) 063521 [`astro-ph/0610419`] [ɪɴSPIRE].

[35] M. Kalb and P. Ramond, *Classical direct interstring action*, *Phys. Rev.* **D 9** (1974) 2273 [ɪɴSPIRE].

[36] A. Vilenkin and T. Vachaspati, *Radiation of Goldstone bosons from cosmic strings*, *Phys. Rev.* **D 35** (1987) 1138 [ɪɴSPIRE].

[37] N. Turok and P. Bhattacharjee, *Stretching cosmic strings*, *Phys. Rev.* **D 29** (1984) 1557 [ɪɴSPIRE].

[38] E.P.S. Shellard, *Cosmic string interactions*, *Nucl. Phys.* **B 283** (1987) 624 [ɪɴSPIRE].